

**A LINE-FOCUS TRANSDUCER SYSTEM FOR PROPERTY CHARACTERIZATION
OF MATERIALS FABRICATED BY ADDITIVE MANUFACTURING**

by

Xuande Zhang

Bachelor of Science, Xiamen University, 2011

Submitted to the Graduate Faculty of
Swanson School of Engineering in partial fulfillment
of the requirements for the degree of
Master of Science

University of Pittsburgh

2015

UNIVERSITY OF PITTSBURGH
SWANSON SCHOOL OF ENGINEERING

This thesis was presented

by

Xuande Zhang

It was defended on

April 6, 2015

and approved by

Qing-Ming Wang, Ph.D., Professor

Department of Mechanical Engineering and Materials Science

Patrick Smolinski, Ph.D., Associate Professor,

Department of Mechanical Engineering and Materials Science

Williams S. Slaughter, Ph.D., Associate Professor,

Department of Mechanical Engineering and Materials Science

Thesis Advisor: Qing-Ming Wang, Ph.D., Professor,

Department of Mechanical Engineering and Materials Science

Copyright © by Xuande Zhang

2015

A LINE-FOCUS TRANSDUCER SYSTEM FOR PROPERTY CHARACTERIZATION OF MATERIALS FABRICATED BY ADDITIVE MANUFACTURING

Xuande Zhang, M.S.

University of Pittsburgh, 2015

Nondestructive evaluation methods have been studied increasingly in recent years. Due to its characteristics, such as high-resolution, low cost, etc., ultrasonic testing has become one of the most used NDE methods. Furthermore, principles of ultrasonic have also provided a novel tool for materials property characterization.

A line-focus PVDF ultrasonic wave transducer was designed, fabricated, and tested. Numerous concepts of ultrasonic wave near boundary were discussed. Rayleigh (Surface) wave, which plays a vital role in this work, has been investigated and tested by the PVDF transducer. With tested Rayleigh wave velocities, elastic constant (Young's Modulus) could be derived. Conclusions could be drawn through comparison since the relationship between elastic constants and Rayleigh wave was well studied.

In addition to that, a short introduction of additive manufacturing was made briefly. Two additive manufacturing methods, laser-based and water-based were mentioned. Since properties of finished sample of additive manufacture still remain uncertainty. Samples fabricated in these

two methods have been tested as well as standard part. The comparisons between these samples have been done in the end.

The major goals of this work are to: 1) study the basic knowledge of Rayleigh wave properties and its applications; 2) develop an acoustic understanding of material fabricated in different methods; and 3) verify the relationship between elastic constants and surface wave velocity.

TABLE OF CONTENTS

| | |
|--|-------------|
| NOMENCLATURE..... | XIII |
| ACKNOWLEDGEMENT..... | XIV |
| 1.0 INTRODUCTION..... | 1 |
| 2.0 BACKGROUND | 2 |
| 2.1 NONDESTRUCTIVE EVALUATION..... | 2 |
| 2.1.1 Ultrasonic Testing..... | 3 |
| 2.2 PIEZOELECTRIC MATERIAL | 4 |
| 2.3 ADDITIVE MANUFACTURING..... | 5 |
| 3.0 FUNDAMENTALS OF ULTRASOUND | 7 |
| 3.1 BULK WAVES..... | 7 |
| 3.1.1 Longitudinal Wave and Shear Wave..... | 7 |
| 3.1.2 Governing Equations for Fluid | 9 |
| 3.1.2.1 Equation of Motion | 9 |
| 3.1.2.2 Constitutive Equations | 10 |
| 3.1.2.3 Wave Equation | 11 |
| 3.1.3 Incident Angle and Snell’s Law..... | 12 |
| 3.1.3.1 First Critical Angle | 14 |
| 3.1.3.2 Second Critical Angle (Rayleigh Angle)..... | 14 |

| | | |
|---------|--|----|
| 3.2 | RAYLEIGH WAVE (SURFACE WAVE) | 15 |
| 3.2.1 | Mathematical Expression | 17 |
| 3.2.1.1 | Impedance | 21 |
| 3.2.1.2 | Attenuation | 22 |
| 3.2.2 | Leaky Surface Wave | 22 |
| 3.3 | ELASTIC CONSTANTS AND SURFACE WAVE | 24 |
| 4.0 | LINE-FOCUS TRANSDUCER SYSTEM | 26 |
| 4.1 | BACKGROUND OF ULTRASONIC CHARACTERIZATION | 26 |
| 4.2 | DESIGN | 28 |
| 4.3 | MANUFACTURE | 32 |
| 4.4 | V(Z) CURVE | 38 |
| 4.4.1 | Green’s function | 40 |
| 5.0 | EXPERIMENT RESULTS AND ANALYSIS | 43 |
| 5.1 | STANDARD STAINLESS STEEL 420 SAMPLE | 46 |
| 5.2 | ROUGHNESS | 52 |
| 5.3 | ADDITIVE MANUFACTURING PRODUCTS | 59 |
| 5.3.1 | ExOne M-Flex | 59 |
| 5.3.2 | LENS 450 Laser 3D Printer | 65 |
| 6.0 | CONCLUSION AND FUTURE WORK | 67 |
| 6.1 | CONCLUSION | 67 |
| 6.2 | FUTURE WORK | 67 |
| 6.2.1 | Different Piezoelectric Material | 67 |
| 6.2.2 | Anisotropic Material Characterization | 68 |

| | |
|---------------------------|-----------|
| APPENDIX A | 69 |
| BIBLIOGRAPHY | 70 |

LIST OF TABLES

| | |
|---|----|
| Table 2-1 Approximate Frequency Ranges | 3 |
| Table 4-1 Acoustic Properties of Different Materials..... | 36 |
| Table 5-1 Stainless Steel 420 Composition Sheet from McMaster-Carr..... | 43 |
| Table 5-2 Experiment Results..... | 52 |
| Table 5-3 Experimental Elastic Constant | 52 |
| Table 5-4 Elastic Constants Calculated from Roughness Testing Results | 58 |
| Table 5-5 Elastic Constants Calculated by Ultrasonic Wave Testing Method..... | 65 |
| Table 5-6 Elastic Constant Results of Laser Additive Manufacturing | 66 |
| Table 6-1 Piezoelectric Properties of PVDF and Piezoelectric Ceramics | 68 |

LIST OF FIGURES

| | |
|--|----|
| Figure 2-1 Inverse Piezoelectric Effect..... | 4 |
| Figure 3-1 Schematic of Longitudinal Wave..... | 7 |
| Figure 3-2 Schematic of Shear Wave | 8 |
| Figure 3-3 Undeformed Geometry and Deformed Geometry..... | 11 |
| Figure 3-4 Refraction of Wave in Different Media | 12 |
| Figure 3-5 Wave Reflection and Refraction at the Wedge-Steel Interface | 13 |
| Figure 3-6 First Critical Angle..... | 14 |
| Figure 3-7 Second Critical Angle | 15 |
| Figure 3-8 Rayleigh Wave Propagation and Particle Motion follows Elliptical Orbit..... | 17 |
| Figure 4-1 Sketch of Microscope Geometry for Transmission | 26 |
| Figure 4-2 Basic Ingredients of Ultrasonic Equipment | 29 |
| Figure 4-3 Ray Presentation of the Lens Line-Focus Transducer Probing Wave | 30 |
| Figure 4-4 Representation of lens-less line focus transducer probing a liquid/solid interface..... | 31 |
| Figure 4-5 Transducer Assemble | 31 |
| Figure 4-6 Epoxy | 33 |
| Figure 4-7 Schematic of Transducer Fabrication..... | 34 |

| | |
|---|----|
| Figure 4-8 Backing Material Solidified in Aluminum Case..... | 34 |
| Figure 4-9 PVDF with Leads..... | 35 |
| Figure 4-10 Reflection Waveform..... | 37 |
| Figure 4-11 Reflection matched Green’s Function Prediction..... | 38 |
| Figure 4-12 Schematic of Wave Path..... | 39 |
| Figure 4-13 Waveform Simulation [18]..... | 42 |
| Figure 5-1 Waveforms on Time Domain..... | 45 |
| Figure 5-2 Waveforms with an Offset on Time Domain..... | 45 |
| Figure 5-3 Schematic of Different Direction Test..... | 46 |
| Figure 5-4 Standard Stainless Steel 420 Sample at 0° | 47 |
| Figure 5-5 Standard Stainless Steel 420 Sample at 45° | 47 |
| Figure 5-6 Conventional Fabricated Stainless Steel 420 Sample at 90° | 48 |
| Figure 5-7 Conventional Fabricated Stainless Steel 420 Sample at 135° | 48 |
| Figure 5-8 Waveform overlaps of Standard Stainless Steel 420 Sample at 0° | 49 |
| Figure 5-9 Waveform overlaps of Standard Stainless Steel 420 Sample at 45° | 50 |
| Figure 5-10 Waveform overlaps of Standard Stainless Steel 420 at 90° | 50 |
| Figure 5-11 Waveform overlaps of Stainless Steel 420 at 135° | 51 |
| Figure 5-12 2D Analysis on #60 Sample x-axis..... | 53 |
| Figure 5-13 2D Analysis on #60 Sample y-axis..... | 53 |
| Figure 5-14 2D Analysis #320 Sample x-axis..... | 53 |
| Figure 5-15 2D Analysis #320 Sample y-axis..... | 54 |
| Figure 5-16 2D Analysis #1200 Sample x-axis..... | 54 |
| Figure 5-17 2D Analysis #1200 Sample y-axis..... | 54 |

| | |
|--|----|
| Figure 5-18 3D Interactive Display #60 Sample | 55 |
| Figure 5-19 3D Inactive Display #320 Sample..... | 55 |
| Figure 5-20 3D Interactive Display #1200 Sample | 56 |
| Figure 5-21 Sample polished with grinding paper 60..... | 56 |
| Figure 5-22 Sample polished with grinding paper 320..... | 57 |
| Figure 5-23 Sample polished with grinding paper 1200..... | 57 |
| Figure 5-24 Wave Velocities on Different Roughness Surface Comparison | 58 |
| Figure 5-25 Illustration of Partical Sintering | 59 |
| Figure 5-26 A kind of Temperature Profiles during Sintering[29]..... | 60 |
| Figure 5-27 2D Analysis x- axis on Sample 150 mins at 1375 degree..... | 60 |
| Figure 5-28 2D Analysis y-axis on Sample 225 mins at 1375 degree..... | 61 |
| Figure 5-29 3D Interactive Display of Sample 150 mins at 1375 degree..... | 61 |
| Figure 5-30 2D Analysis x- axis on Sample 225 mins at 1375 degree..... | 62 |
| Figure 5-31 2D Analysis y- axis on Sample 225 mins at 1375 degree..... | 62 |
| Figure 5-32 3D Interactive Display of Sample 225 mins at 1375 degree..... | 63 |
| Figure 5-33 Sintering Process at 1350 degree for 300 mins..... | 64 |
| Figure 5-34 Sintering Process at 1375 degree for 225 mins..... | 64 |
| Figure 5-35 Waveforms of Laser Sample with offset..... | 65 |
| Figure 5-36 Comparison between Laser Additive Manufacturing Sample and Standard Sample | 66 |

NOMENCLATURE

| | |
|----------------|---|
| Z | Acoustic Impedance |
| ω | Angular Frequency |
| f | Frequency |
| ρ | Density |
| R | Radius |
| D | Focus Length |
| c | Velocity |
| Z | Acoustic Impedance |
| ν | Poisson's Ratio |
| E | Young's Modulus |
| α_{CR} | Critical Angle |
| α_{1CR} | First Critical Angle |
| α_{2CR} | Second Critical Angle (Rayleigh Critical Angle) |

ACKNOWLEDGEMENT

This research would never be done without supports from kind people. Here I would like to present my sincere gratitude to them.

Firstly, I would like to thank my advisor, Professor Qing-Ming Wang, for his patient and meticulous through my research. Furthermore, I would like to express my thanks to my committee members: Dr. William Slaughter and Dr. Patrick Smolinski, for their time and help to make this thesis better.

Secondly, my thanks to my research partner, Yuxiang Wang, for his knowledge and experience, being a great help in this research. Also, thank my research group member, Huiyan Wu, Hongfei Zu, Qiuyan Li, Rongjie Liang, Zheng Min, they have been supportive all the time.

In addition, my gratitude to Yu Zhou, Yongsen Rong and Sin Chien Siw from material science for helping me to prepare all the test samples.

Finally, I would like to thank my parents for their support and encouragement.

Thanks to them all.

1.0 INTRODUCTION

The development of the aperture lens-less line-focus ultrasonic transducer ultrasonic testing began in the late 1920s. Fundamental physics, geometrics and wave optics were copied in the original design, then ultrasonic transducers have been redesigned and improved by a large number of investigators.

A few basic NDE methods, ultrasonic wave propagation characteristics, piezoelectric material, and overview of additive manufacturing were done aperture lens-less line-focus ultrasonic transducer. Upon those knowledge, a lens-less line-focus acoustic system could be designed, fabricated, and tested.

Chapter 3 is dedicated to explain wave interpretation and analysis methodology. Governing equations, reflection/refraction, propagation of surface wave will be explained explicitly. Beyond that, how the elastic constants related to ultrasonic velocities will be derived.

Chapter 4 will show all the details of design, manufacturing, and testing of the ultrasonic system.

In Chapter 5, the wave velocity results are collected, analyzed. Material isotropy, surface roughness are taken into consideration for thorough analysis.

Conclusions and future work will be drawn in Chapter 6.

2.0 BACKGROUND

2.1 NONDESTRUCTIVE EVALUATION

In the past few decades, the processing of material has kept improving. With a growing demand of high-level properties for materials, high-accuracy and rapid-result testing evaluation methods have been more discovered and studied. All the industrial material evaluations could be classified in two major categories: nondestructive evaluation (NDE) and destructive evaluation. Nondestructive evaluation, or nondestructive testing (NDT) is a process of detection, measurement, and evaluation of discontinuities in raw material or finished parts, without leaving any damage on them or changing physical properties of them. In contrast, traditional destructive evaluation are much easier to carry out, yield more information and are easier to interpret than NDE. Destructive testing is more suitable for mass-produced, which means the cost of destroying a particular amount is negligible [1].

Nondestructive testing methods could be classified under physical principles that form the basis for each method. NDT methods are named according to these physical principles. The most common NDT methods are listed below [1]:

- Ultrasonic Testing (UT);
- Acoustic emission testing (AE);
- Penetrant testing (PT);
- Magnetic particle testing (MT);
- Eddy current testing (ET);

- Radiographic testing (RT);
- Visual Testing (VT);
- Thermal infrared testing (TIR);

Among these testing methods above, ultrasonic testing (UT) is a relatively new branch in science and industry. Since its accuracy and versatility, ultrasonic wave testing is the first or second choice of most discontinuities, such as: planar surface rupture on test surface, subsurface planar rupture near test surface, internal volumetric discontinuity, geometric imperfection on opposite surface, etc.

2.1.1 Ultrasonic Testing

Ultrasound is a kind of oscillating pressure wave with a relatively high frequency. Investigator define it inasmuch its frequency is beyond human hearing which is between 20 Hz to 20 kHz.

Table 2-1 Approximate Frequency Ranges

| Infrasound | Acoustic | Ultrasound |
|------------|---------------|------------|
| 0~20 Hz | 20 Hz ~20 kHz | 20 kHz ~ |

Ultrasonic NDE uses high-frequency acoustic/elastic waves to evaluate objects without affecting their integrity or performance. High-frequency gives a high resolution meanwhile comes with a high cost. As a result, in different areas, i.e., industry, medical care, selection of ultrasound frequency would be an important part. Beside frequency, number of wave modes, such as Rayleigh wave, Lamb wave, etc. are well employed in different applications due to their characteristics respectively.

2.2 PIEZOELECTRIC MATERIAL

Acoustic transducers that generated acoustic wave provide significant advantages, relative to comparable electromagnetic devices. They are compact, simple, and highly reliable; and they require minimal energy to produce a high level of sound [2]. Ultrasonic energy is generated in most cases by a piezoelectric element. In other word, the effectiveness of most ultrasonic testing very much depends on the selection of the piezoelectric transducers, which generates, transmit and receive ultrasonic waves and thus provide a large amount of information about the existing reflectors in the test samples.

Piezoelectric effect is a phenomenon among some certain materials which generate an electric charge in response to applied mechanical press. This effect, called direct piezoelectric effect, is well applied on sensors. Meanwhile in piezoelectric transducers, mechanical vibration energy is generated when electrical energy applied. This phenomenon is called ‘inverse piezoelectric effect’.

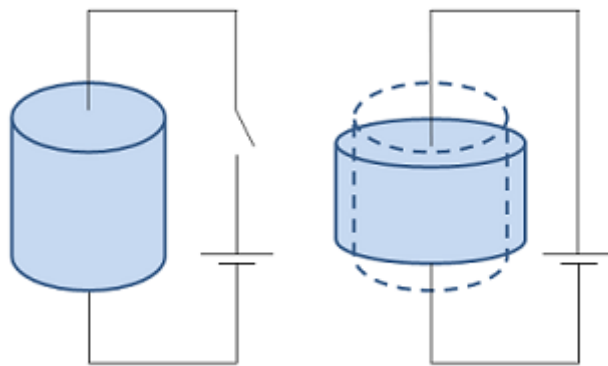


Figure 2-1 Inverse Piezoelectric Effect (www.comsol.com)

Different inverse piezoelectric modes exist in a variety of materials. Thickness mode, which is performed on PVDF film, was used in this work. Some fundamentals of thickness mode are presented below.

2.3 ADDITIVE MANUFACTURING

Traditional manufacturing of steel includes several processes, i.e., casting, forming, machining, and joining. Traditional manufacturing has its own characteristics, for instance, casting has strong flexibility and adaptability to produce parts of different materials and in different shapes. However, traditional manufacturing cost a lot due to some processes require particular temperature and pressure, etc. Furthermore, long-term term traditional producing process from raw materials to final products, which rises the risk of non-uniform properties and wastes materials [3].

Additive manufacturing is a process with a brand new concept to produce a three dimensional part from a digital model designed through software without process planning. In additive manufacturing, a digital model of the desired part designed by a three-dimensional (3D) computer-aided designed (CAD) software is converted into surface tessellation (.stl) file. With stl file is then transferred into an additive manufacturing system for analysis and set-up. Let us put it simple: engineers utilize computer-aided designed software to ‘cut’ all the models in to pieces (layers), then use additive manufacturing technology to build it layer by layer using chemical

liquid binder or high-energy laser. Through additive manufacturing technology, much more complex geometry would be obtained with less effort.

In this article, two different additive manufacturing product were tested. One is from ExOne company using chemical liquid binder as glue to build up objects. The other one is from Optomec using laser to make object solid. Even though additive manufacturing technology has a bunch of advantages, some technical defects exist still, such as low physical properties, shrinkage, hollow, crack, etc. Ultrasonic wave testing on additive manufacturing parts involved in this work. From this method, elastic constants were achieved. Comparison between traditional method and additive manufacturing were done.

3.0 FUNDAMENTALS OF ULTRASOUND

3.1 BULK WAVES

3.1.1 Longitudinal Wave and Shear Wave

Solids, liquids, and gaseous media are characterized by their elasticity of volume, that is, their ability to retain the volume, but the solid, in addition has an elasticity of shape, that is, its ability to retain the shape. The shear elasticity of solid materials is a result of this feature. Any attempt of a volume expansion or compression, as well as a shifting of adjacent layers using variable force, will result in an occurrence of an elastic oscillation. Thus, so-called tensile-compression oscillations can be created in all media except within a vacuum. Waves with this type of particle motion are longitudinal waves [1]. (Particle motion is parallel to the direction of propagation.)

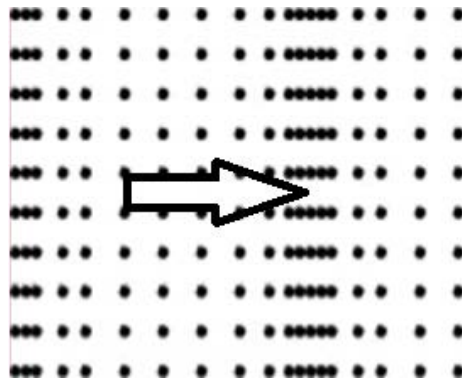


Figure 3-1 Schematic of Longitudinal Wave (www.nde-eg.org)

The other type of wave, which particle movement is normal to the wave propagation direction, is called shear or transvers wave. In most cases, shear waves (S-waves) are propagated at an angle to a test object surface. However, when necessary, S-waves can be generated perpendicular to a test object surface, using a special transducer and couplant. Both longitudinal and shear waves are bulk waves.

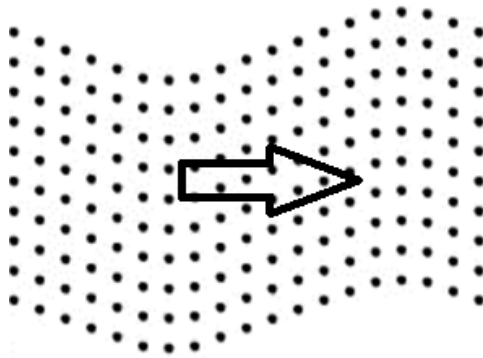


Figure 3-2 Schematic of Shear Wave (www.nde-eg.org)

There are two types of S-waves: vertically polarized shear waves (SVs) and horizontally polarized shear waves (SHs). In the vertically polarized shear waves, particles oscillate in a plane perpendicular to the test object surface. In the horizontally polarized shear waves, particles oscillate in a plane oriented at the refracted angle to the test object surface. In the other word, the particle movement direction of vertical shear wave is normal to the particle movement direction in horizontal shear wave. Vertically polarized shear waves are commonly used in ultrasonic testing.

Longitudinal waves are generated by straight beam transducers. Vertically polarized shear waves are generated by a probe comprising a transducer and a wedge which we would

primarily discuss in this article. Horizontally polarized shear waves, as a rule, are generated by an electromagnetic acoustic transducer (EMAT).

People start describing characteristics of the wave transmitting with the basic relation in wave description:

$$f\lambda = c \quad (3.1)$$

Which means value of sound velocity is product of frequency and wavelength. In next sections, some principles of wave would be discussed in order to carry out experiment design.

3.1.2 Governing Equations for Fluid [4]

3.1.2.1 Equation of Motion

In NDE, because all the displacement and velocities involved are very small, we could have a relationship in a volume V of an ideal compressible fluid in motion:

$$\int_V \mathbf{f}(\mathbf{x}, t) dV(\mathbf{x}) - \int_S p(\mathbf{x}_s, t) \mathbf{n}(\mathbf{x}_s) dS(\mathbf{x}_s) = \int_V \rho(\mathbf{x}, t) \mathbf{a}(\mathbf{x}, t) dV(\mathbf{x}) \quad (3.2)$$

Which $p(\mathbf{x}_s, t)$ is the pressure in the fluid at any point \mathbf{x} and time t and relate the forces acting in V and on its surface S to the rate of change of momentum, \mathbf{x}_s is arbitrary point on the surface S of V whose outward normal is the unit vector \mathbf{n} . Vector quantities \mathbf{f} and \mathbf{a} are the body force (force/unit volume) and acceleration of the fluid, respectively, and $\rho(\mathbf{x}, t)$ is the fluid density.

After applying the divergence theorem to the first term in Eq.(3.2) to convert it into a volume integral, we have

$$\int_V [-\nabla p(\mathbf{x}, t) + \mathbf{f}(\mathbf{x}, t) - \rho \mathbf{a}(\mathbf{x}, t)] dV(\mathbf{x}) = 0 \quad (3.3)$$

where ∇ is the vector gradient operator. The integral balance expressed by Eq.(3.3) must be true for an arbitrary volume V , so the integrand itself must be zero at every point \mathbf{x} in the fluid, leading to the differential equation:

$$-\nabla p(\mathbf{x}, t) + \mathbf{f}(\mathbf{x}, t) = \rho \mathbf{a}(\mathbf{x}, t) \quad (3.4)$$

Since all waves in NDE applications involve very small displacements and velocities, we can assume the density is the same as its value ρ_0 in the undisturbed state, for instance, $\rho = \rho(\mathbf{x})$, and the acceleration $\mathbf{a} = \partial^2 \mathbf{u} / \partial t^2$, where \mathbf{u} is the displacement vector. Under these conditions Eq.(3.4) becomes

$$-\nabla p + \mathbf{f} = \rho_0 \partial^2 \mathbf{u} / \partial t^2 \quad (3.5)$$

3.1.2.2 Constitutive Equations

To turn Eq.(3.5) into an equation in only a single variable, such as pressure, we must relate the pressure to the motion \mathbf{u} through the material properties of the fluid. Such a relationship is called a constitutive equation. For an ideal compressible fluid, pressure is proportional to the divergence of the displacement vector, also known as the dilatation of the fluid:

$$p = -\lambda \nabla \cdot \mathbf{u} \quad (3.6)$$

The proportionality constant λ is the bulk modulus of the fluid.

The dilation term in Eq.(3.6) can be given an explicit physical meaning. To see this consider a small element of fluid as shown in figure below

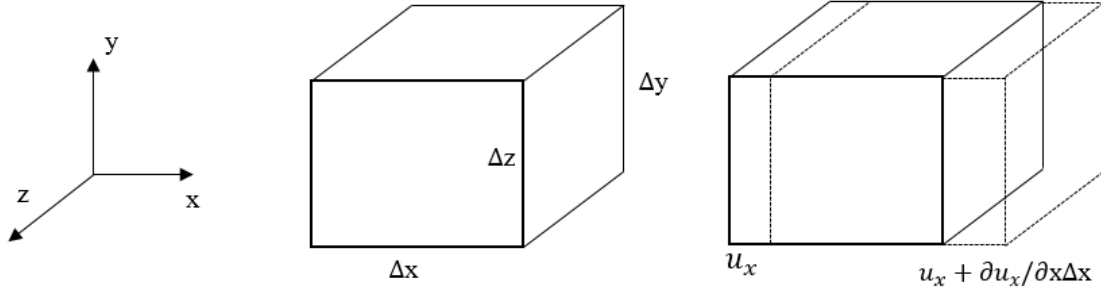


Figure 3-3 Undeformed Geometry and Deformed Geometry

If this element is given a displacement component in the x direction u_x only and this displacement is spatially varying, then the volume change ΔV_x produced by this x-displacement is to first order given by:

$$\Delta V_x = \frac{\partial u_x}{\partial x} \Delta V \quad (3.7)$$

where $\Delta V = \Delta x \Delta y \Delta z$ is the original volume of our small element. Similarly we can have ΔV_y and ΔV_z .

When all three displacements are present simultaneously, then to first order we have

$$\Delta V_x + \Delta V_y + \Delta V_z = \left(\frac{\partial u_x}{\partial x} + \frac{\partial u_y}{\partial y} + \frac{\partial u_z}{\partial z} \right) \Delta V \quad (3.8)$$

So that:

$$\nabla \cdot \mathbf{u} = \frac{\Delta V_x + \Delta V_y + \Delta V_z}{\Delta V} \quad (3.9)$$

3.1.2.3 Wave Equation

If we take the divergence of both sides of Eq.(3.5), we can use the constitutive relationship Eq.(3.6) to obtain

$$\nabla^2 p + f = \frac{\rho_0}{\lambda} \frac{\partial^2 p}{\partial t^2} \quad (3.10)$$

where $\nabla^2 = \nabla \cdot \nabla$ is the laplacian operator and $f = -\nabla \cdot \mathbf{f}$ is a scalar body force term. Since it is the three-dimensional inhomogeneous wave equation for the pressure, we can rewrite it as:

$$\nabla^2 p - \frac{1}{c^2} \frac{\partial^2 p}{\partial t^2} + f = 0 \quad (3.11)$$

where the quantity $c = \left(\frac{\lambda}{\rho}\right)^2$ is the speed of the sound in fluid.

3.1.3 Incident Angle and Snell's Law

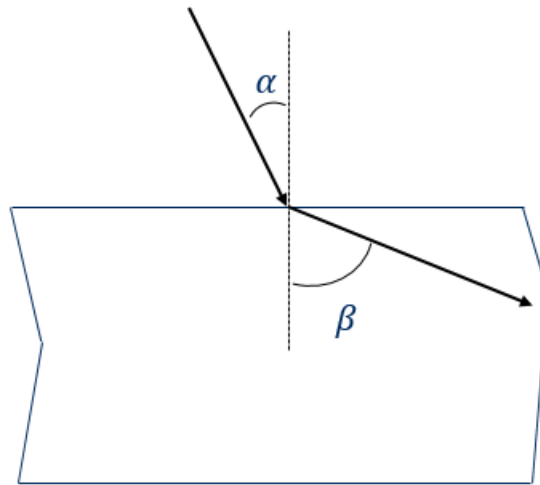


Figure 3-4 Refraction of Wave in Different Media

When ultrasonic wave propagates through the interface between two different media, the travel path changes somehow as shown above. Snell's law states that the ratio of the sines of the angles

of incidence and refraction is equivalent to the ratio of phase velocities in the two media, or equivalent to the reciprocal of the ratio of the indices of refraction:

$$\frac{\sin \alpha}{\sin \beta} = \frac{c_1}{c_2} \quad (3.12)$$

where α and c_1 are incidence angle and wave velocity in the first media, θ_2, c_2 are the refraction angle and wave velocity in the second media.

In most NDE cases, engineers do not only cast ultrasonic wave normal to samples but with different angles. As I mentioned before, vertical shear waves are generated by an acoustic probe with a wedge. Here is the reason behind this: beside the laws of reflection and refraction, a phenomenon of wave transformation or mode conversion has to be considered, according to which one mode of waves can be converted to another. The incidence beam is longitudinal wave with an angle. At the boundary of two different media, wave mode change occurs as shown below.

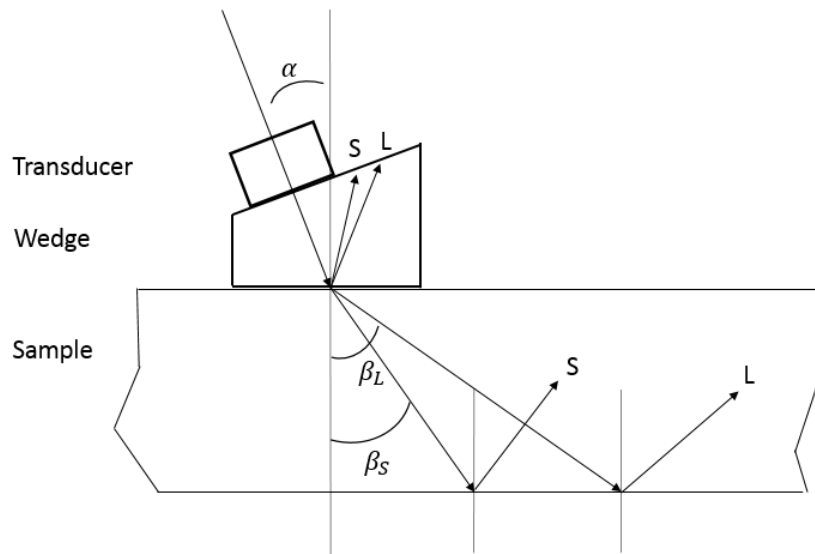


Figure 3-5 Wave Reflection and Refraction at the Wedge-Steel Interface [1]

3.1.3.1 First Critical Angle

In the wedge-steel case, according to Snell's law, at a particular angle, which known as the first critical angle α_{1CR} , the longitudinal wave L should propagate along the front surface of a test object, and only shear wave S should propagate inside the test object at a calculated refracted angle β .

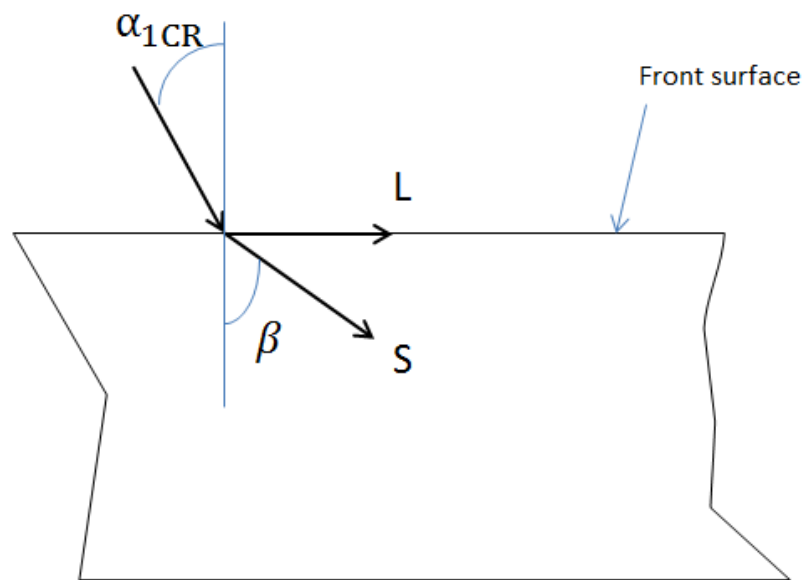


Figure 3-6 First Critical Angle

3.1.3.2 Second Critical Angle (Rayleigh Angle)

If the angle of incidence is further increased to the second critical angle α_{2CR} , the S-wave will transform into a surface wave, propagating, for instance, along the metal-air interface. Beyond this angle, according to the law, no wave will be transmitted into the material of the test objects.

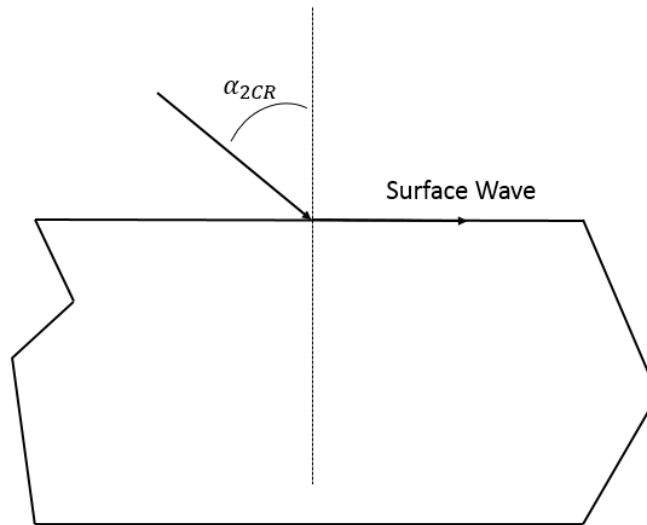


Figure 3-7 Second Critical Angle

Since Rayleigh wave was important in my work. In next section, fundamentals of Rayleigh wave will be discussed.

3.2 RAYLEIGH WAVE (SURFACE WAVE)

In addition to bulk waves, a number of other wave types are commonly used in ultrasonic testing: surface or Rayleigh waves, normal or Lamb waves, and several other types of guided waves. In 1885, the English scientist Lord Rayleigh demonstrated theoretically that waves can be propagated along the plane boundary between an elastic half-space and a vacuum or sufficiently rarefied medium (i.e. air), where the amplitude of the waves decays rapidly with depth [5]. These waves were named Rayleigh or surface waves later and have been studied in details in

seismology [6]. The application of ultrasonic Rayleigh wave provides the solution of a number of conceptually important problems. For instance, it has become versatility applicable for components of any shape and size. Therefore, the volume (longitudinal and transvers) waves used for ultrasonic testing by propagation in solids whose dimension along the wave front is larger than the wavelength have been inapplicable for the testing of thin-walled samples, or for the surface layer of a sample (since the reflection from a defect is masked by reflection from the surface). Ultrasonic Rayleigh and Lamb waves remove these limitations at once.

A surface wave is a combination or superimposition of longitudinal and vertically polarized shear waves travelling the surface of a relatively thick solid material penetrating to a depth of one wavelength. Therefore Surface wave combines both a longitudinal and transvers motion to create an elliptic orbit motion as shown in the image below. A surface wave's maximum energy is concentrated on the surface of the test object where the waves are generated and rapidly decrease with depth. Therefore, surface-breaking discontinuities are detectable with these waves.

The major axis of the ellipse is perpendicular to the surface of the solid. As the depth of an individual atom from the surface increases the width of its elliptical motion decreases.

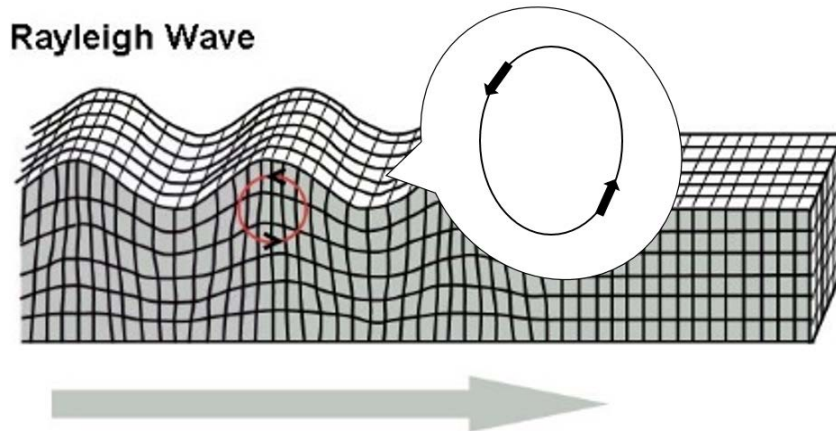


Figure 3-8 Rayleigh Wave Propagation [http://www.geo.mtu.edu/UPSeis/rayleigh_web.jpg] and Particle Motion follows Elliptical Orbit

3.2.1 Mathematical Expression

Having the two distinct wave speeds $c_p \equiv c_l \equiv c_1$ and $c_s \equiv c_t \equiv c_2$, given in terms of the Lamé constants as:

$$c_p = \sqrt{\frac{\lambda + 2\mu}{\rho}}$$

$$c_s = \sqrt{\frac{\mu}{\rho}}$$

Then in an elastic solid, disturbances associated with the scalar potential ϕ travel with wave speed c_p . These disturbances are called P-waves, compressional waves, primary waves, longitudinal (L) waves, etc. In contrast disturbances associated with the vector potential ψ travel with the wave speed c_s ; these are called S-waves, shear waves, secondary waves, tangential (T)

waves, etc. Both P- and S- waves are called P- and S- bulk waves because they represent disturbances propagating in the bulk or elastic solid. If we consider the ratio of these two waves speeds, $\kappa = c_p/c_s$, this ratio can be written as a function of Poisson's ratio only:

$$\kappa = \sqrt{\frac{2(1 + \nu)}{1 - 2\nu}}$$

For the displacement, we can decompose the displacement vector into a scalar potential ϕ and a vector potential ψ (through the Helmholtz decomposition theorem [7]).

$$\mathbf{u} = \nabla\phi + \nabla \times \psi \quad (3.13)$$

Consider the plane stress-free surface of an elastic solid (Figure 3-10). Lord Rayleigh sought solutions to the equation of motion that represented traveling waves confined primarily to a region near the surface. Since Rayleigh wave is mixtures of both longitudinal and shear wave motions satisfying the governing equations for displacement potentials given by (for harmonic wave of time dependency of $\exp(-i\omega t)$):

$$\frac{\partial^2\phi}{\partial x^2} + \frac{\partial^2\phi}{\partial y^2} + \frac{\omega^2}{c_p^2}\phi = 0 \quad (3.14)$$

$$\frac{\partial^2\psi}{\partial x^2} + \frac{\partial^2\psi}{\partial y^2} + \frac{\omega^2}{c_s^2}\psi = 0 \quad (3.15)$$

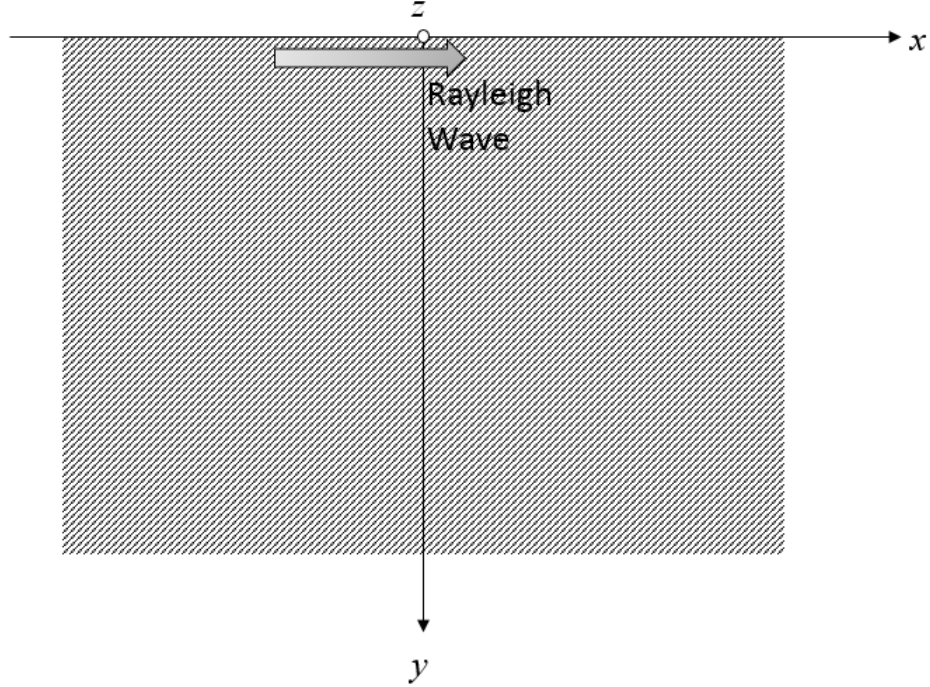


Figure 3-9 Liquid-Solid interface

Since we are looking for disturbances that decay in amplitude away from the surface, we assume disturbances of a form similar to what we found for inhomogeneous waves:

$$\phi = A \exp(-\alpha y) \exp[ik(x - ct)] \quad (3.16)$$

$$\Psi = B \exp(-\beta y) \exp[ik(x - ct)] \quad (3.17)$$

where c is the wave speed of the propagating wave $k = \omega/c$ and α and β are unknown exponential decay coefficients. Using these expressions in the equations of motion Eq.(3.14) and Eq.(3.15), has

$$\left[-k^2 + \alpha^2 + \left(\frac{\omega^2}{c_p^2} \right) \right] A \exp(-\alpha y) \exp[ik(x - ct)] = 0 \quad (3.18)$$

$$\left[-k^2 + \beta^2 + \left(\frac{\omega^2}{c_s^2} \right) \right] B \exp(-\beta y) \exp[ik(x - ct)] = 0 \quad (3.19)$$

Which give α and β explicitly as:

$$\alpha = \left(k^2 - \frac{\omega^2}{c_p^2} \right)^{1/2} = |k| \left(1 - \frac{c^2}{c_p^2} \right)^{1/2} \quad (3.20)$$

$$\beta = \left(k^2 - \frac{\omega^2}{c_s^2} \right)^{1/2} = |k| \left(1 - \frac{c^2}{c_s^2} \right)^{1/2} \quad (3.21)$$

When solutions in Eq.(3.16) and Eq.(3.17) exist and these are confined to the surface (so α and β are both real), then as Eq.(3.20) and Eq.(3.21) shows, we must have $c < c_s < c_p$, which means surface wave must be slower than a bulk shear wave in the same material.

Using Eq.(3.16) and Eq.(3.17) in expressions for displacement u_x and u_y and τ_{xy} gives

$$u_x = (ikAe^{-\alpha y} - \beta B e^{-\beta y})e^{ik(x-ct)} \quad (3.22)$$

$$u_y = (-\alpha A e^{-\alpha y} - ikB e^{-\beta y})e^{ik(x-ct)} \quad (3.23)$$

$$\tau_{yy} = \mu[(2k^2 - k_s^2)Ae^{-\alpha y} + 2ik\beta B e^{-\beta y}]e^{ik(x-ct)} \quad (3.24)$$

$$\tau_{xy} = \mu[-2ik\alpha e^{-\alpha y} + (\beta^2 + k^2)B e^{-\beta y}]e^{ik(x-ct)} \quad (3.25)$$

To determine an explicit value for the wave speed c , the stress-free boundary condition at the surface $y = 0$ must be satisfied, i.e.:

$$(\beta^2 + k^2)A + 2ik\beta B = 0 \quad (3.26)$$

$$-2ik\alpha A + (\beta^2 + k^2)B = 0 \quad (3.27)$$

Here $k_s = \omega/c_s$, we use the relationship $2k^2 - k_s^2 = \beta^2 + k^2$, which produce homogeneous equations for amplitudes A and B. For nontrivial solution to exist for this set of equations, the determinant of the matrix of coefficients must vanish, giving

$$(\beta^2 + k^2)^2 - 4k^2\alpha\beta = 0 \quad (3.28)$$

Equivalently when common frequency terms are eliminated

$$\left(2 - \frac{c^2}{c_s^2}\right)^2 - 4\left(1 - \frac{c^2}{c_p^2}\right)^{-1/2} \left(1 - \frac{c^2}{c_s^2}\right)^{1/2} = 0 \quad (3.29)$$

A detailed analysis of its properties was talked by J. Achenbach [8] shows that there is always a real root of this equation $c = c_R$ that satisfies $c_R < c_s$, guaranteeing that such surface waves always exist. A simple equation that give good fit to the roots is

$$c_R = \frac{0.862 + 1.14\nu}{1 + \nu} c_s \quad (3.30)$$

With the boundary conditions fix the ratio of ϕ and ψ , we would have a secular equation for c ,

$$4\left(\frac{c_T}{c}\right)^2 \left[1 - \left(\frac{c_T}{c}\right)^2\right]^{1/2} \left[\left(\frac{c_T}{c_L}\right)^2 - \left(\frac{c_T}{c}\right)^2\right]^{1/2} + [1 - 2\left(\frac{c_T}{c}\right)^2]^2 = 0 \quad (3.31)$$

which is ‘‘Rayleigh Equation’’. One root $c = c_R$ that gives real positive values of $\gamma_{R,T}$ is always present, with the property

$$0 < c_R < c_T < c_L$$

varying approximately from $0.87c_T$ to $0.96c_T$ as ν varies from 0 to 0.5. The corresponding Rayleigh waves are (nondispersive) plane inhomogenous waves, undamped in their direction of propagation along the surface (x), and damped normal to the boundary (z). They are a couple compressional-shear system, propagating with unique velocity c_R along x , elliptically polarized in the xz planewith a degree depending on z .

3.2.1.1 Impedance

Reflection of acoustic wave’s incident on a planar interface between two isotropic media is most easily considered in terms of impedances. Acoustic characteristic impedance is defined as minus the ratio of traction to particle displacement velocity,

$$Z \equiv -\frac{\sigma_T}{\partial u / \partial r} \quad (3.32)$$

The traction σ_T is the vector force per unit area acting on a surface. The unit of impedance is the rayl. The impedance is equal to the product of the density ρ of a medium and the velocity v of a given wave propagating in it; this is how impedance is usually calculated, $Z \equiv \rho v$ ($1 \text{ Rayl} = 1 \frac{N \cdot s}{m^3} = 1 \frac{ba \cdot s}{cm} = 1 \frac{g}{s \cdot cm^2}$). In MKS units, 1 Rayl equals 1 pascal-second per meter ($Pa \cdot s \cdot m^{-1}$), or equivalently 1 newton-second per cubic meter ($N \cdot s \cdot m^{-3}$). In SI base units, that is $Kg \cdot s^{-1} \cdot m^{-2}$.

3.2.1.2 Attenuation

Energy attenuation coefficient for the leaky Rayleigh wave is

$$\alpha_R = \frac{1}{P_R} \frac{dP_R}{dx} = \frac{\rho_{liquid} c_w}{\rho_{solid} c_R \lambda} \text{ cm}^{-1} \quad (3.33)$$

From the equation above, we could know the attenuation per wavelength of the leaky wave is given by the ratio of the acoustic impedances. In most cases, α_R is relatively low (around 0.10) so that the wave is attenuated to zero over the distance of 10 wavelengths.

3.2.2 Leaky Surface Wave [8][9][10]

If the vacuum bounding the plane elastic half-space is replaced by a liquid or by another solid, the Rayleigh wave description need to be modified. Early studies on this subject are due to Love (1991) and Stoneley (1924); the corresponding generalized Rayleigh waves are also known as “Stoneley waves”.

Application of the boundary conditions on the liquid-solid interface determines ϕ and ψ , we could have the secular equations for c ,

$$\begin{aligned}
& 4\left(\frac{c_T}{c}\right)^2\left[1 - \left(\frac{c_T}{c}\right)^2\right]^{1/2}\left[\left(\frac{c_T}{c_L}\right)^2 - \left(\frac{c_T}{c}\right)^2\right]^{1/2} + \left[1 - 2\left(\frac{c_T}{c}\right)^2\right]^2 \\
& = -\frac{\rho_l}{\rho_s}\left[\frac{(c_T/c_L)^2 - (c_T/c)^2}{(c_T/c_L)^2 - (c_T/c)^2}\right]^{1/2}
\end{aligned} \tag{3.34}$$

is satisfied. This agrees with the Rayleigh equation if the density ρ_l of the liquid is negligible as compared to the density ρ_s of the solid. There will be a root c that tends to c_R as $\rho_l \rightarrow 0$; this root is always complex (Brekhovskikh, 1960). Calling c_R' , the velocity of this “generalized Rayleigh wave”, we have [11]:

$$c_R < c_R' < c_T < c_L$$

The wave is complex, thus decays as it propagates along the surface. Moreover, the propagation vectors are inclined towards the boundary, so that energy flows across the interface (leaky wave): hence the attenuation along the propagation direction.

Leaky surface waves have been proven to provide a well-studied tool in acoustic microscopy. They are generated by ultrasound incident at the critical Rayleigh angle. Leaky Rayleigh waves are attenuated due to transmission of the component normal to the surface into the liquid.

The phase velocity V_R of leaky Rayleigh waves has been calculated and tabulated by Viktorov [11] for different values of Poisson’s Ratio and density Ratio. The effect is typically very small; for instance, for an average interface, the parameters plotted by Viktorov are $c_S/c_L = 5$ and $\rho_1/\rho_2 = 0.5$, leading to $c_R/c_{LSAW} \approx 1.001$.

The attenuation factor for the leaky Rayleigh wave has also been derived by Viktorov. Compared to velocity, this is very important. It was proven that surface acoustic wave has normal and tangential components of displacement.

3.3 ELASTIC CONSTANTS AND SURFACE WAVE

Since the leaky Rayleigh wave at a liquid/solid interface loses energy in the liquid, the wave number k is a complex quantity, expressed in terms of the wave speed V_R and the attenuation coefficient α as

$$k = \frac{\omega}{V_R} + i\alpha \quad (3.35)$$

where ω is the angular frequency.

Consider a leaky Rayleigh wave propagates on an isotropic solid half-space in contact with a liquid half-space, the complex-valued wave number k satisfies the following characteristic equation given by Viktorov [11]:

$$4k^2qs - (k^2 + s^2)^2 - i\frac{\rho_W q k_T^4}{\rho q_W} = 0 \quad (3.36)$$

Where $q = \sqrt{k^2 - k_L^2}$, $s = \sqrt{k^2 - k_T^2}$, $q_W = \sqrt{k_W^2 - k^2}$ and $k_j = \frac{\omega}{v_j} : j = L, T, W$, ρ is the density of solid, ρ_W is the density of liquid and tis wave speed is V_W , V_L and V_T are the longitudinal and transvers wave speed, respectively.

Using the measured speed V_R and V_L and the density ρ with the speed V_W and density ρ_W of water, we can obtain the attenuation coefficient α and the transverse wave speed V_T from the

condition that the real and imaginary parts of Eq.(3.36) are zero (Lee et al., 1995). The Poisson's ratio ν , Young's modulus E , the shear modulus G , and the bulk modulus K of the solid are given by (Ristic, 1983)

$$\nu = \frac{\lambda}{2(\lambda + \mu)},$$

$$E = \frac{\mu(3\lambda + 2\mu)}{\lambda + \mu},$$

$$G = \mu,$$

$$K = \lambda + \frac{2}{3}\mu,$$

where $\lambda = \rho(c_L^2 - 2c_S^2)$ and $\mu = \rho c_S^2$.

The longitudinal wave speed of material was gained from defocus technique, with knowing Rayleigh wave speed of stainless steel.

4.0 LINE-FOCUS TRANSDUCER SYSTEM

4.1 BACKGROUND OF ULTRASONIC CHARACTERIZATION

The first mechanically scanning acoustic microscope was designed by Lemons and Quate in 1973 [12], the applications have been widely studied to detect microscopically the variation of acoustic properties of different materials in the fields of biological science, solid mechanics science. In 1979, Lemons and Quate invented an acoustic microscopy with mechanical scanning. This new instrument formed a single spherical surface at a solid liquid interface.

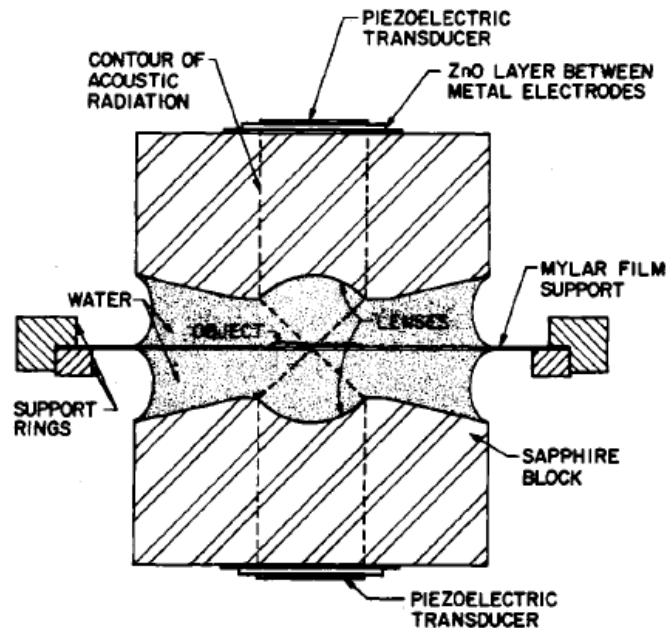


Figure 4-1 Sketch of Microscope Geometry for Transmission [12]

Almost three decades, a large number of investigators have improved our knowledge of both surface and subsurface acoustic microscopy so today it is one of the most versatile materials characterization methods that available to people. It has been proven that the output of piezoelectric transducer varies obviously with change of the distance between probe and sample [13] [14]. The record of this output has been called the $V(z)$ curve and it is a function of the distance of z . Since those $V(z)$ curves are unique and characteristic of solid materials, it has been shown that the reflection acoustic microscope system, operating in the non-scanning mode, provides for the determination of acoustic properties in solid materials [12] [15].

In later 1980s, the very first generation of line-focus ultrasonic wave transducer was developed by Kushibiki and Chubachi [16] [17]. In their design, the basic idea of the line-focus ultrasonic transducer was use of a lens for focusing planar waves from a transducer onto a sample to obtain a $V(z)$ curve, which is record of the echo-interference amplitude V versus the distance z between the lens and the sample. The interference occurs between the leaky surface wave and the direct reflected wave in a bone-burst mode of operation. The material property measurements are based on analyzing the $V(z)$ curves. An increasing number of types of ultrasonic wave transducers were invented later, for instance, V-groove lens, the slit-aperture lens, the butterfly transducer and other transducer designs.

In this paper, much work are extension of Dan Xiang's Rayleigh wave characterization [18]. A large aperture ultrasonic wave transducer has been used to determine material properties, such as leaky surface wave velocity, elastic constant.

Applications of the acoustic microscope system using a highly focused beam could be divided broadly into two classes to detect microscopic as well as macroscopic acoustic properties

of materials; viz., acoustic imaging measurements in the scanning version and quantitative measurements in the non-scanning version. Latter one has a better resolution when high frequency wave applied.

4.2 DESIGN

Quantitative material characterization by acoustic microscopy has a widespread technique for the nondestructive evaluation. We monitor the amplitude of the transducer output voltage V as a function a spacing z from specimen toward lens, or the $V(z)$ curve. When the transducer is focused on the sample surface, a single echo pulse will be received. If the transducer is moved toward the sample ('defocusing') a distance z , the waveform will separate into two pulses. In J. Kushibiki's and H. Ishiji's work, a relatively high frequency (100 MHz) transducer was use which has a low penetration depth. High frequency tone-bursts provide a high spatial resolution capability, but also result in a high system cost. This system is operating in the relatively low frequency range of 10 MHz to 30 MHz (Maximum frequency of the Pulser & Receiver is 30 MHz). Dealing with common practical measurements concerned with macroscopic rather than microscopic material properties is not necessary.

Figure below shows basic ingredients of an ultrasonic equipment.

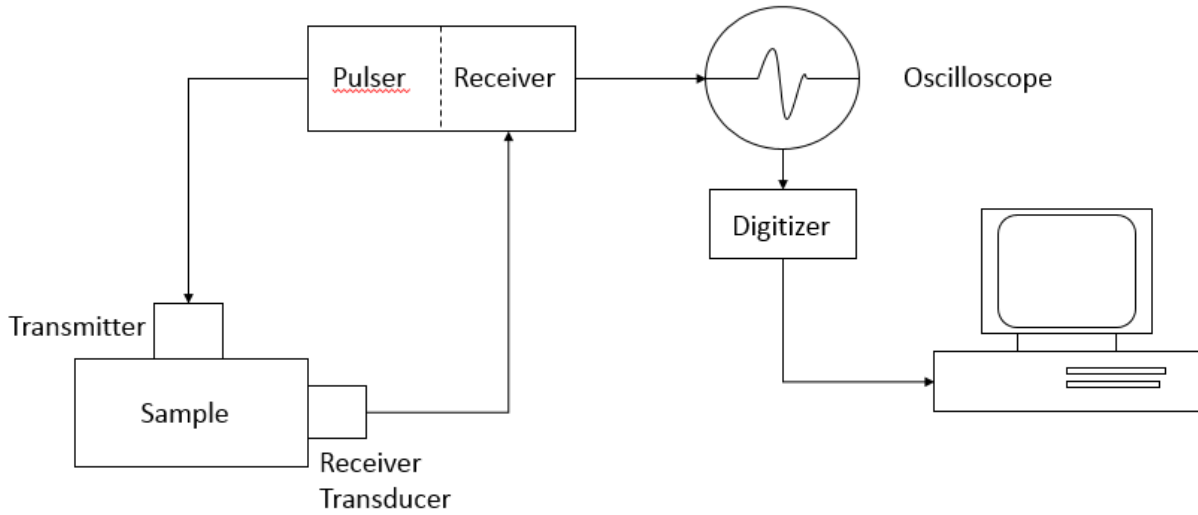


Figure 4-2 Basic Ingredients of Ultrasonic Equipment

In the past century a large number of investigators, i.e., invented, tested, and improved lens acoustic microscopes [12] [15] [17] [21] [22]. People attach the transducer behind a highly-machined lens, which usually is sapphire, to generate ultrasonic wave. The conventional acoustic microscopic designed by J. Kushibiki and H. Ishiji well applied a PVDF as ultrasonic generation element and a sapphire as lens to focus the ultrasonic wave (Figure 4-2).

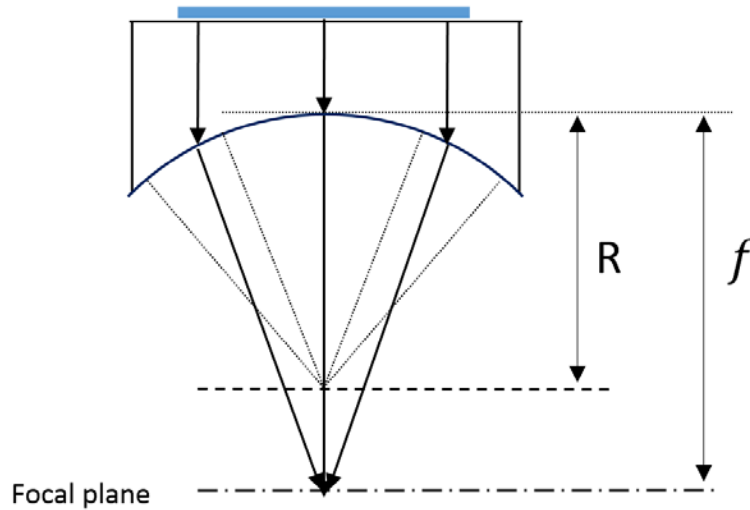


Figure 4-3 Ray Presentation of the Lens Line-Focus Transducer Probing Wave

The acoustic microscope illustrated in Figure 4-2 consists of a longitudinal wave transducer attached on a sapphire rod-lens coupled through a liquid (water) to an object surface. The longitudinal waves are focused by the wide angle lens at a distance $f = Rn_a/(n_a - 1)$ below the top of the lens. n_a is the acoustic refractive index. The reflected waves from the object surface travel back to the transducer through the lens and produce an output voltage.

However, ultrasonic wave loses energy in water, and mathematical expression in sapphire lens probe was more complex. Concave transducer which focuses the beam became a better solution in experiment. Due to the flexibility and low acoustic impedance, commercial PVDF film is ideal as an active element for line-focus transducers. Therefore, in Dan Xiang's work back in 1996, a small PVDF was attached to a concave transducer to generate ultrasonic wave. My ultrasonic transducer is much like an extension of work done by Dan Xiang. In my work, transducer applied a concave high acoustic impedance backing to build a different transducer to focus ultrasonic wave immediately. The ultrasonic wave incident at a particular angle to generate

leaky surface wave at the interface of liquid and solid. This line-focus transducer can use a wave representation as shown in Figure 4-3 and the assembly procedure is shown in Figure 4-4.

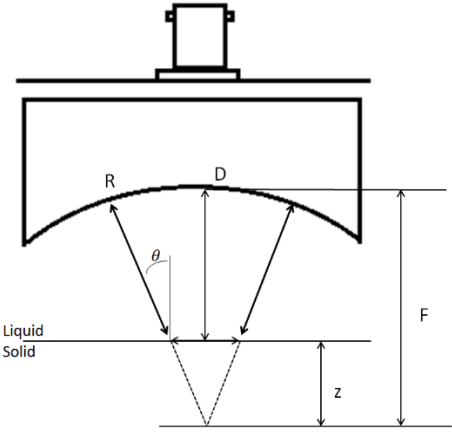


Figure 4-4 Representation of lens-less line focus transducer probing a liquid/solid interface

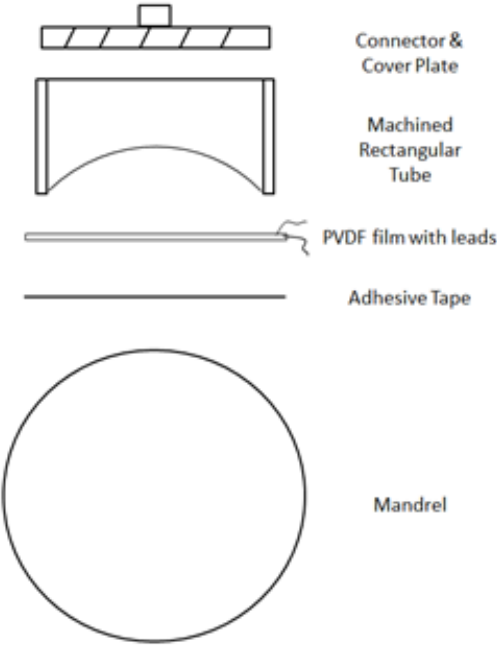


Figure 4-5 Transducer Assemble

Here we use aluminum as the case material since its relatively high acoustic impedance (Table 2, 17.5 Mrayl) and low cost. The rectangular aluminum case will be machined to the required curvature at one end and flat at the other (top) end, with mixture of tungsten powder and epoxy loaded. Also, we use an aluminum tube as the mandrel, with a rectangular PVDF film (with leads) affixed to the convex surface of the mandrel with adhesive tape. Upon curing, the transducer is removed from the mandrel and the adhesive tape removed from the surface of the transducer. Finally, the electrical leads from the PVDF film are soldered to the connector, and a cover plate is sealed to the top of the transducer.

In previous design of surface-wave acoustic microscope by J. Kushibiki and H. Ishiji, the piezoelectric element was attached to a flat backing material, then a sapphire lens was used to focus all the ultrasonic wave to a focal point. Furthermore, the sapphire lens will scatter (negative lens) the reflection back to the pvdf element.

4.3 MANUFACTURE

At this time, we tried to deduce the errors caused by the lens and have more specific results. In the design of the transducer, the choice of backing material should be considered of the acoustic impedance and cost. At this time, a multipurpose aluminum rectangular tube (1/8'' Wall Thick, 1-3/4'' Height, 3-1/2'' Width) fabricated by McMaster-Carr was used as the transducer case. The PVDF element will be attached to a cylindrical (concave) backing material which would focus the wave directly. Here we need to consider the acoustic impedance of the backing material. Also, to make a smooth cylindrical inner surface, an aluminum tube has been used as mandrel.

Here we select tungsten as the backing material cause its high acoustic impedance and low cost. Then epoxy (Devcon, No.14310) was used as adhesive to make a mixture with tungsten powder (Alfa Aeso. -325 mesh, 99.9% metal basis) at a weight ratio of 1:2.



Figure 4-6 Epoxy

After 2 hours, the epoxy solidified which make the PVDF attach to it firmly. Attach it to the stepping machine.

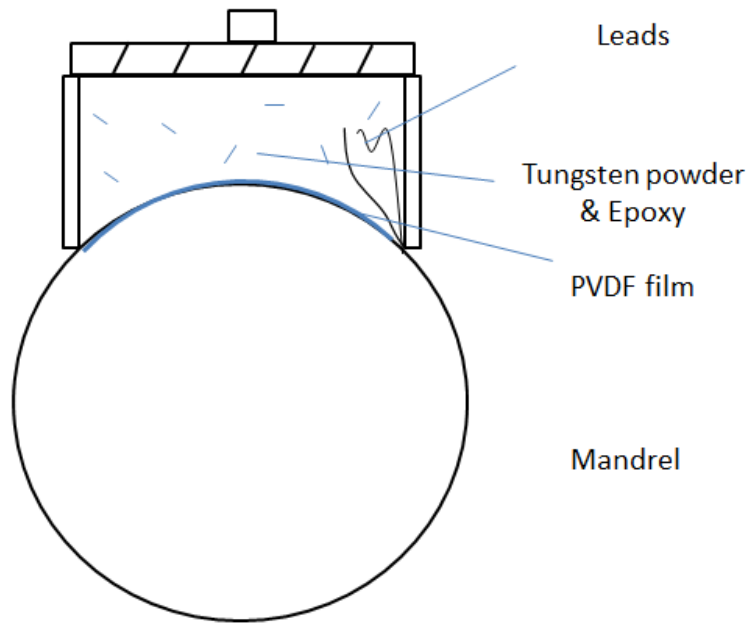


Figure 4-7 Schematic of Transducer Fabrication[18]

Intimately attach the case and the aluminum mandrel, filled it with mixture, vertical placed it for 6 hours, the backing material became firm solid.

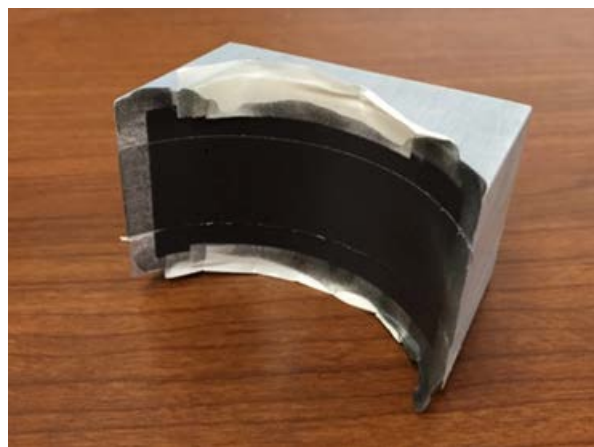


Figure 4-8 Backing Material Solidified in Aluminum Case



Figure 4-9 PVDF with Leads

The rectangular PVDF film (6cm*1.25cm, thickness is 42um, with leads, fabricated by NEG) is affixed to the central of the backing material carefully. Dynamic method was employed to determine its thickness. At the lead part, covered the leads with hot glue to secure it waterproof.

Table 4-1 Acoustic Properties of Different Materials

| Material | Acoustic Properties | | | |
|-------------|----------------------------------|----------------------------------|-------------------------------------|------------------------------------|
| | L-wave velocity, <i>mm/μs</i> | S-wave velocity, <i>mm/μs</i> | Density, <i>g/cm³</i> | Acoustic impedance, <i>ryal</i> |
| Aluminum | 6.42 | 3.04 | 2.70 | 17.5 |
| Epoxy Resin | 2.6-2.7 | 1.1-1.2 | 1.21-1.25 | 2.7-3.5 |
| Tungsten | 5.2 | 2.9 | 1.0 | 101 |
| Water | 1.49 | | 1.0 | 1.49 |

The other parts of this system are an ultrasonic pulser/receiver (Olympus 5072PR) and an oscilloscope (Agilent Technologies, 4034A).

The transducer should be designed for short-pulse broadband operation due to increase measurement resolution in the time domain. Three principal matching parameters require attention for an efficient design: (I) mechanically matching the backing material to the piezoelectric element, (II) mechanically matching the piezoelectric element to the coupling liquid, and (III) electrically matching the piezoelectric to the pulser/receiver network.

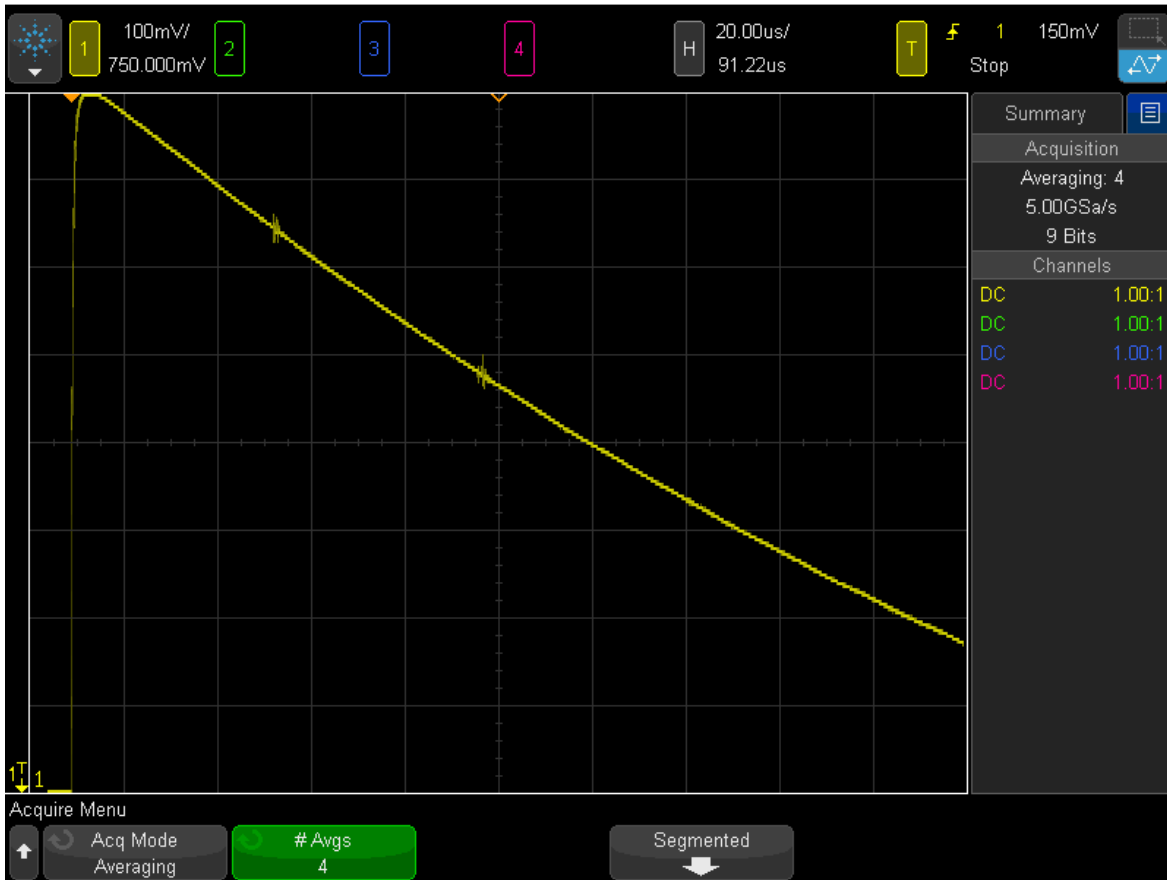


Figure 4-10 Reflection Waveform

We selected stainless steel sample to test. At random distance within defocus distance, we had a figure with several different reflections which highly match the 2-D Green's Function.

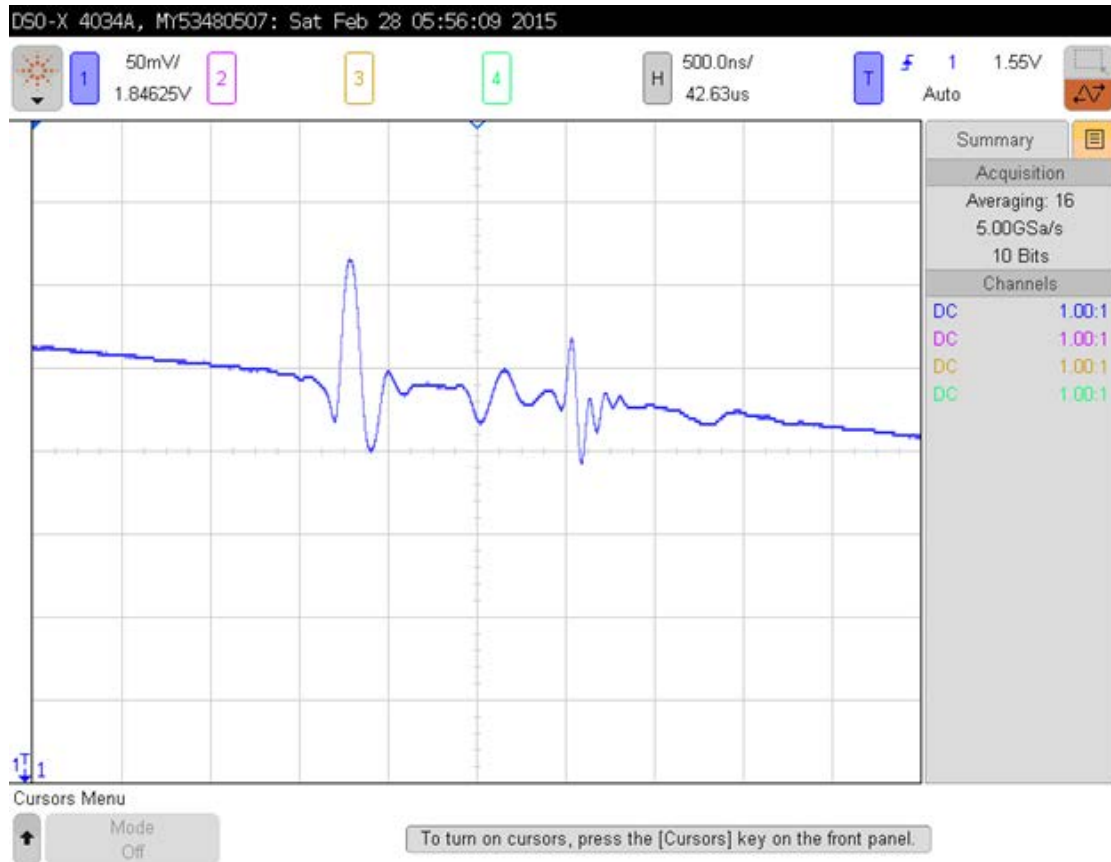


Figure 4-11 Reflection matched Green's Function Prediction

4.4 V(Z) CURVE

We monitor the amplitude of the transducer voltage and record it as $V(z)$ in order to distinguish this displacement along the axis of the beam from the lateral scanning that is used to record conventional acoustic micrographs. The z coordinate is measure from the focal point and positive values correspond to lens-object spacings greater than the focal length.

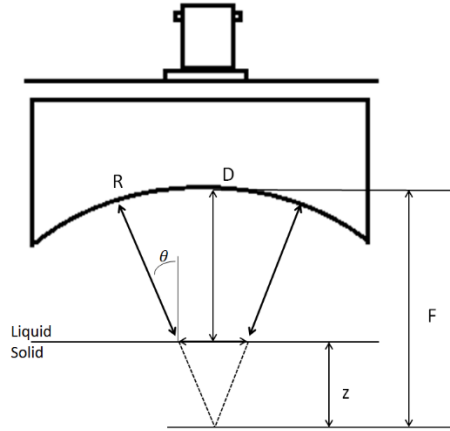


Figure 4-12 Schematic of Wave Path

The arrival time of the leaky surface wave can be represented as

$$t = \frac{2(1 - \cos \theta)}{c_W} z \quad (4.1)$$

where z is the defocus distance between the focal plane and the sample surface, c_W is the longitudinal wave speed of the coupling fluid, and θ is the Rayleigh critical angle given by

$$\theta = \sin^{-1} \left(\frac{c_W}{c_R} \right) \quad (4.2)$$

with c_R the Rayleigh wave speed in the sample.

The slope of this distance z as a function of the arrival time t between pulses provides a relationship in terms of the Rayleigh angle θ ,

$$\frac{dz}{dt} = \frac{c_w}{2(1 - \cos \theta)} \quad (4.3)$$

Using this slope relationship and equation above, the leaky wave velocity can be expressed independently of θ ,

$$c_R = \left[\frac{1}{c_w \left(\frac{dz}{dt}\right)} - \frac{1}{4 \left(\frac{dz}{dt}\right)^2} \right]^{-1/2} \quad (4.4)$$

The surface wave velocity v has a functional relationship to the interval Δz of the periodic dips of the $V(z)$ curve, which is given by the following equation:

$$v = v_w [1 - (1 - c_w/2f\Delta z)^2]^{-1/2} = (c_w \cdot f \cdot \Delta z)^{1/2} (1 - c_w/4f\Delta z)^{-1/2} \quad (4.5)$$

Where c_w is the wave velocity in water, viz. $c_w = 1500 \text{ m/s}$, and f is the wave frequency.

4.4.1 Green's function [18]

When the transducer focuses on the sample surface, a single echo pulse will be received. If the transducer is moved toward the object ('defocusing') a distance z , the wave form will separate into two main pulses in the time domain. The first one on the time domain is the direct reflected wave from the top surface of the sample, the second one is the leaky wave generated from the she surface as it propagates.

To quantitatively predict the lens-less line-focus transducer's behavior, a dynamic Green's function analysis is applied. The fundamental three-dimensional Green's function used to model wave behavior at a horizontal liquid/solid interface for a point source and point receiver situated in the liquid is

$$g(X, T) = \frac{1}{2\pi^2} \int_0^X \text{Real} \left[\frac{\frac{R_a - R_b}{R_a + R_b}}{\sqrt{q^2 - 1} \left[-s + \frac{1}{\sqrt{q^2 - 1}} \right] \sqrt{X^2 - s^2}} \right] ds \quad (4.6)$$

* $X = \frac{d}{h}$, $T = tT_w/h$, d is the horizontal distance between the source and the receiver, h is the sum of the source and receiver heights from the interface, and V_w is the velocity in the liquid(water) with sample

$$q = \frac{sT}{T^2 - 1} + i \frac{\sqrt{T^2 - 1 - s^2}}{T^2 - 1} \quad (4.7)$$

$$R_a = 4\sqrt{(\alpha^2 q^2 - 1)(\beta^2 q^2 - 1)} + (\beta^2 q^2 - 2)^2 \quad (4.8)$$

$$R_b = \sigma \beta^4 q^4 \frac{\sqrt{\alpha^2 q^2 - 1}}{\sqrt{q^2 - 1}} \quad (4.9)$$

$$\alpha = \frac{c_w}{c_l}, \quad \beta = \frac{c_w}{c_s}, \quad \sigma = \frac{\rho_w}{\rho_s} \quad (4.10)$$

Where ρ_w and ρ_s are respectively the liquid (water) and solid densities, and V_s and V_l are the shear and longitudinal wave speeds in the solid.

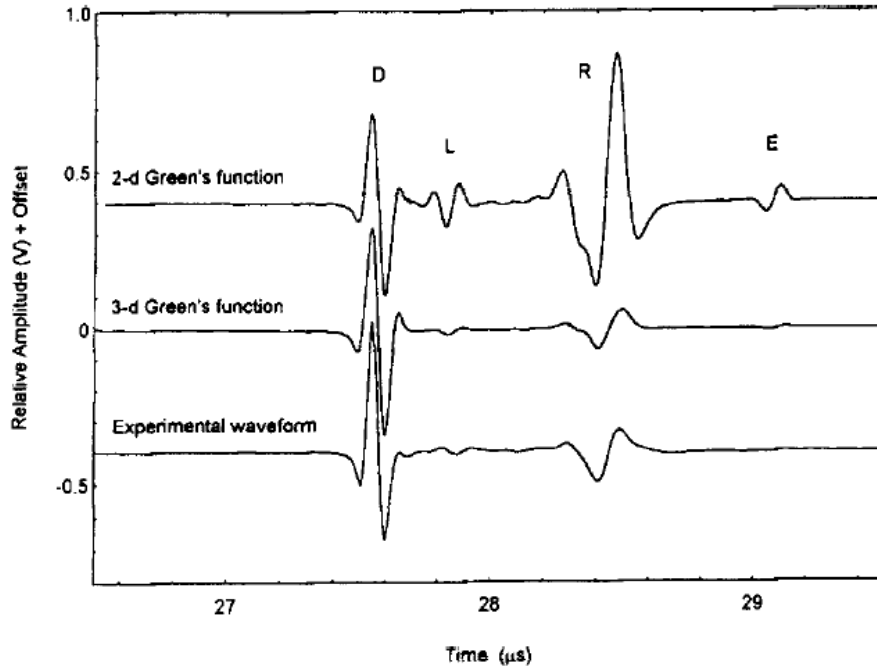


Figure 4-13 Waveform Simulation [18]

5.0 EXPERIMENT RESULTS AND ANALYSIS

In experiments, a stainless steel 420 product (annealed) fabricated by McMaster-Carr was taken as control group. Also, stainless steel 420 samples fabricated by two additive manufacturing machines using different methods will be tested. With experimental wave velocities, elastic constants have been obtained. All the results were obtain under room temperature (25°C). Deionized water was selected as couplant.

Table 5-1 Stainless Steel 420 Composition Sheet from McMaster-Carr

| COMPOSITION | % |
|-------------|---------------|
| Carbon | 0.15 – 0.46 |
| Manganese | 0.40 – 1.00 |
| Vanadium | 0.3 |
| Iron | 82.1 – 87.15 |
| Phosphorus | 0 – 0.04 |
| Sulfur | 0 – 0.03 |
| Silicon | 0 – 1.00 |
| Molybdenum | 0 – 1.00 |
| Chromium | 12.00 – 14.00 |

Also, we have known density $\rho = 7.75 \text{ g/cm}^3$, elastic modulus $E = 200 \text{ GPa}$.¹

We have The SH plate wave has the same velocity as the free transverse wave.

$$c_R = \frac{0.87 + 1.12\mu}{1 + \mu} \sqrt{\frac{E}{\rho} \frac{1}{2(1 + \mu)}} \quad (5.1)$$

Use c_t expression,

$$c_R = c_t \frac{0.87 + 1.12\mu}{1 + \mu} \quad (5.2)$$

We used the directly reflected surface echo as the scope trigger, we achieved a series of waveform traces as a function of position z (Figure). In addition to the prominent leaky surface wave following the directly reflected (triggering) echo, other waves may be observed in the traces such as the leaky skimming longitudinal waves and the sample back-surface echo near 2.3 us. The peak positions of these pulses are searched, plotted, and fitted in figures. From these data, we can simultaneously determine the leaky surface wave velocity, the longitudinal wave velocity, and the sample thickness.

¹ McMaster-Carr

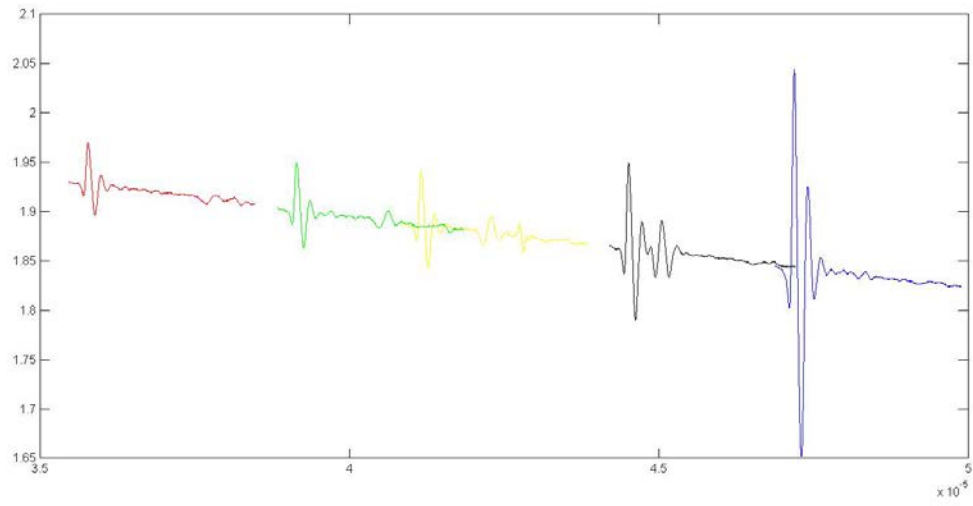


Figure 5-1 Waveforms on Time Domain

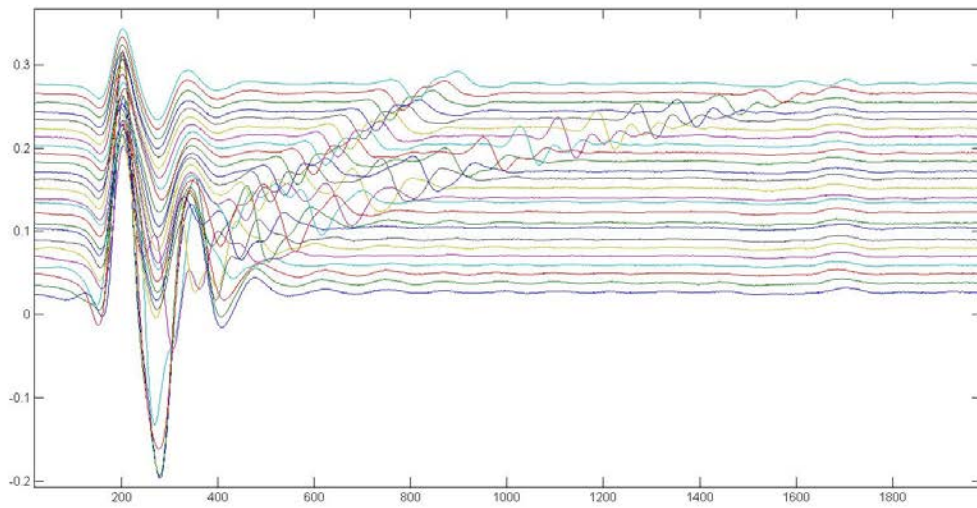


Figure 5-2 Waveforms with an Offset on Time Domain

5.1 STANDARD STAINLESS STEEL 420 SAMPLE

We set the transducer at its own focal length. Then lowered it once every 0.25 mm 20-30 times. In control group testing, for accuracy purpose, Rayleigh wave velocities were tested in four directions (0°, 45°, 90°, 135°).

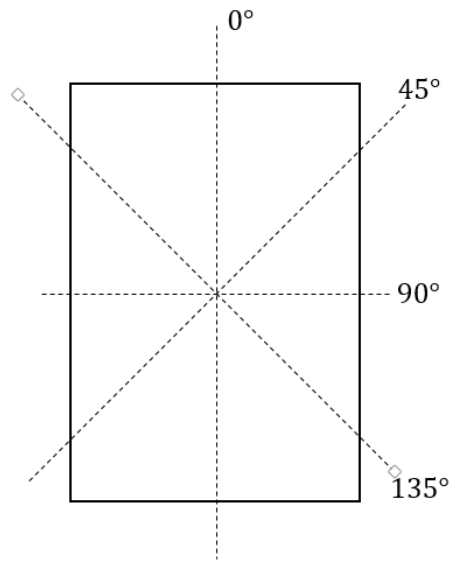


Figure 5-3 Schematic of Different Direction Test

Every series of data was record first and plotted with MatLab. In order to find the slop of $\frac{dv}{dt}$. All the waveforms from one section were plotted on one figure as below.

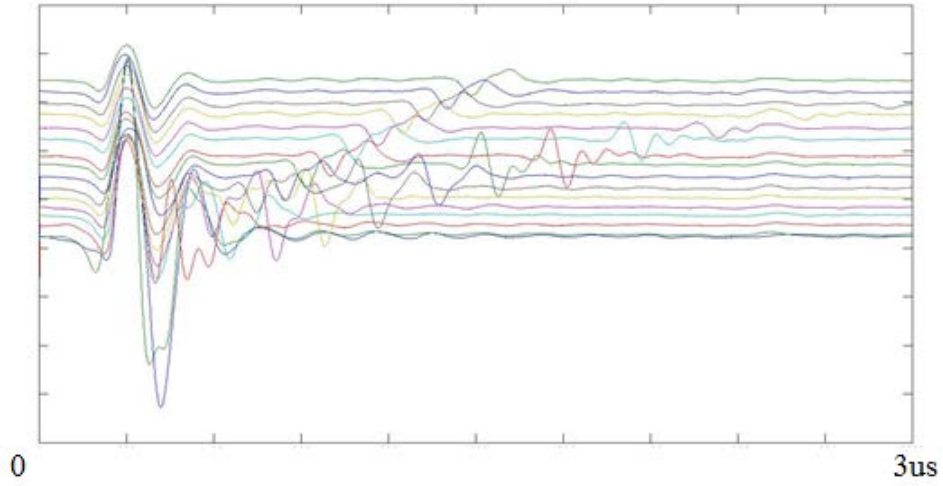


Figure 5-4 Standard Stainless Steel 420 Sample at 0°

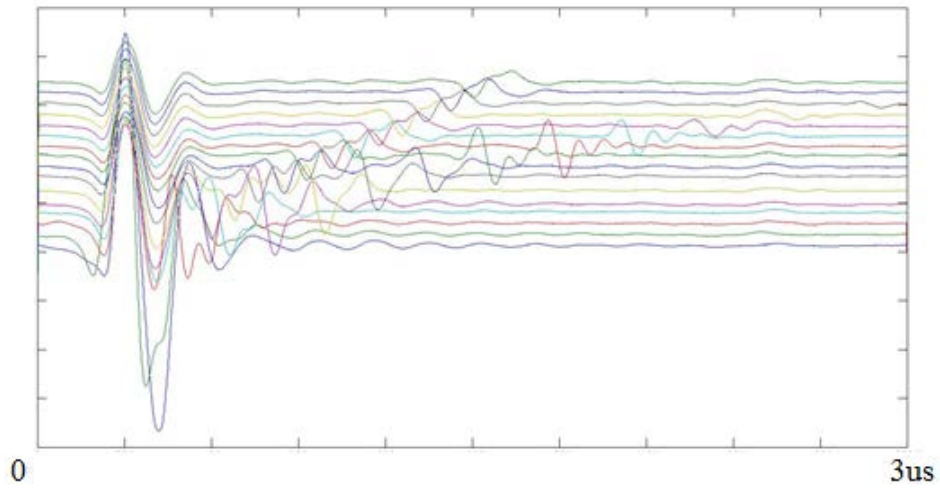


Figure 5-5 Standard Stainless Steel 420 Sample at 45°

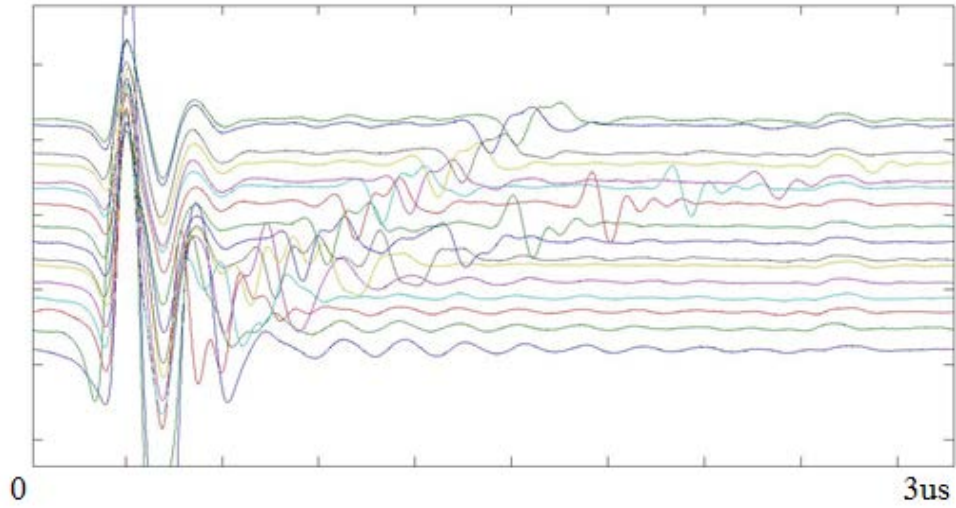


Figure 5-6 Conventional Fabricated Stainless Steel 420 Sample at 90°

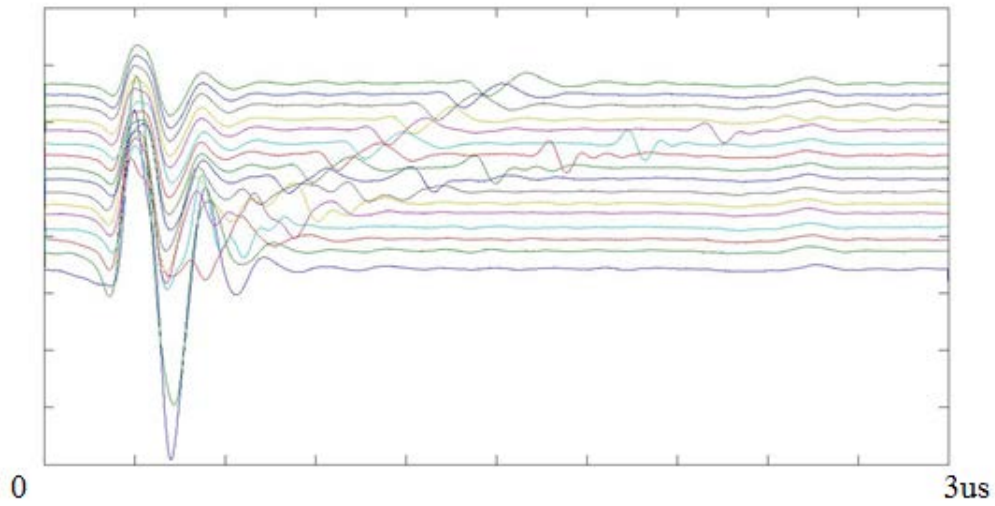


Figure 5-7 Conventional Fabricated Stainless Steel 420 Sample at 135°

Through the figures above, the slop of each series of peaks were drawn and calculated. The slope of this distance z as a function of the arrival time t between pulses provides a relationship in terms of the Rayleigh angle θ discussed before [18]:

$$c_R = \left[\frac{1}{c_W \left(\frac{dz}{dt} \right)} - \frac{1}{4 \left(\frac{dz}{dt} \right)^2} \right]^{-1/2} \quad (5.3)$$

A similar expression for the leaky longitudinal wave velocity can also be readily derived.

If we discard the defocus distance, use all the first peaks as reference, we can also find a wave reflection from the bottom surface. We have a relationship between thickness and travel time easily:

$$\frac{2d}{c_L} = t$$

d : thickness of the stainless steel sample (measured: 6.60 mm), t : travel time in the sample

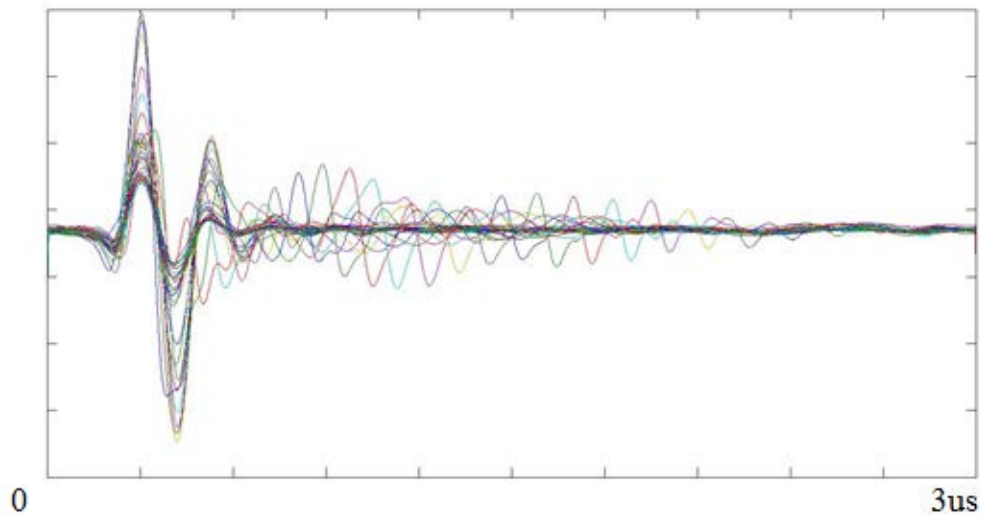


Figure 5-8 Waveform overlaps of Standard Stainless Steel 420 Sample at 0°

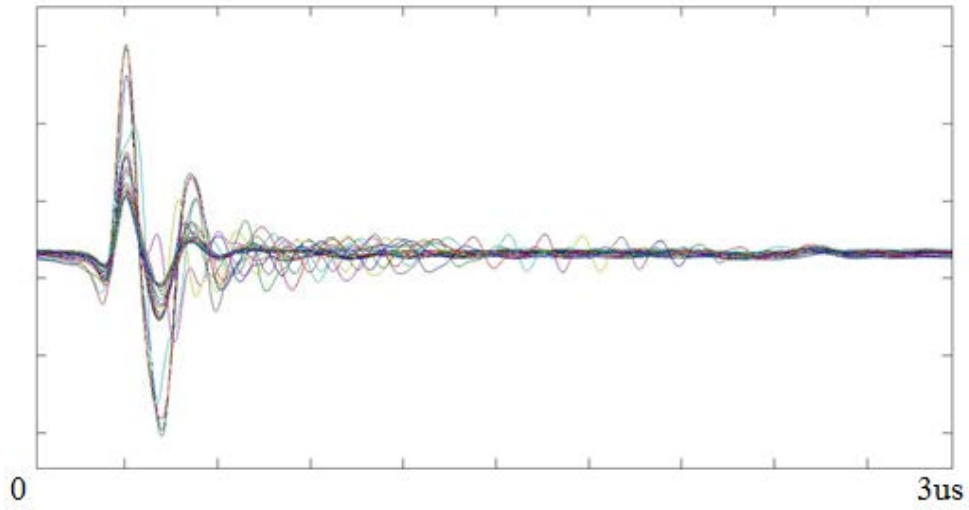


Figure 5-9 Waveform overlaps of Standard Stainless Steel 420 Sample at 45°

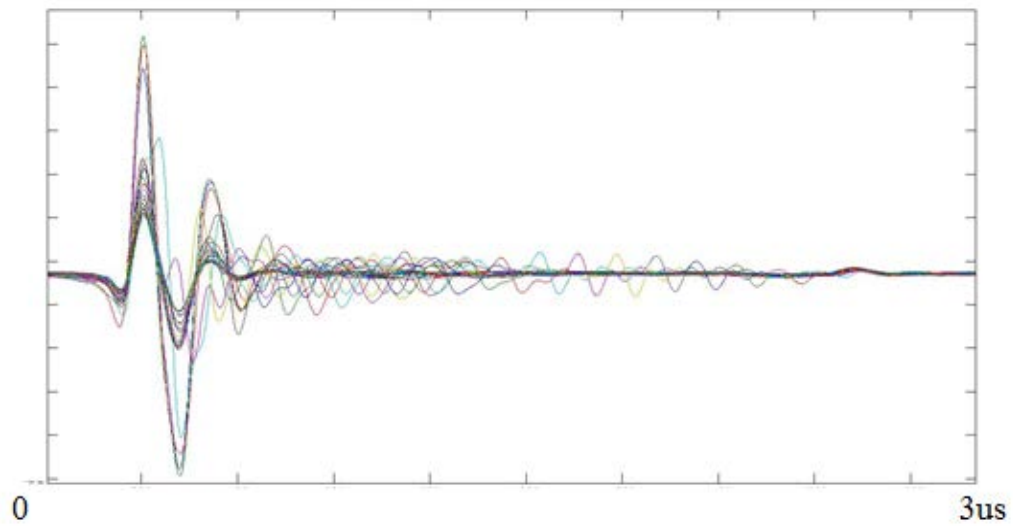


Figure 5-10 Waveform overlaps of Standard Stainless Steel 420 at 90°

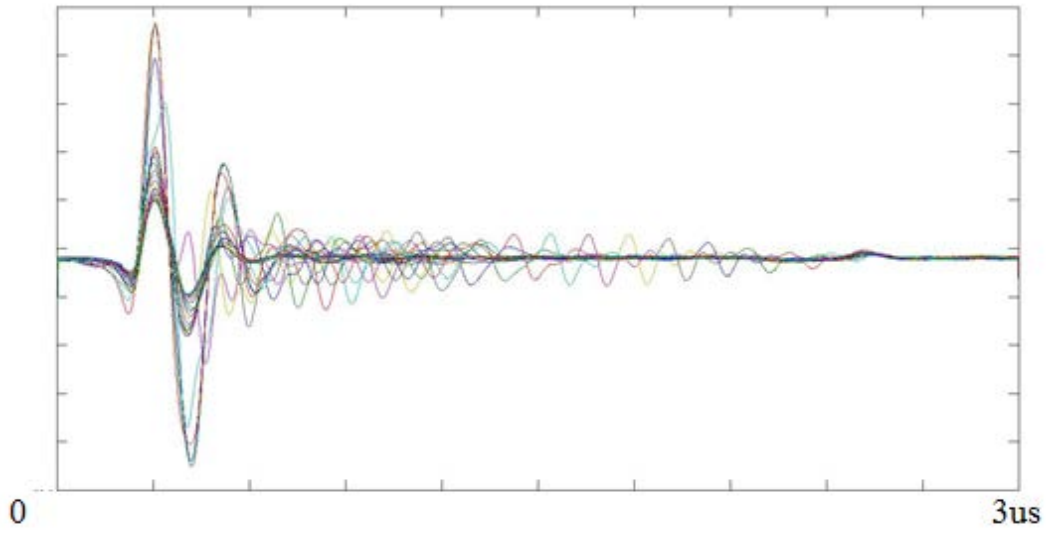


Figure 5-11 Waveform overlaps of Stainless Steel 420 at 135°

Table 5-2 Experiment Results

| (unit: m/s) | 0° | 45° | 90° | 135° | Average |
|-------------------------|------|------|------|------|---------|
| Rayleigh Wave | 2983 | 2970 | 2925 | 2934 | 2923 |
| Shear (Transverse) Wave | 3155 | 3173 | 3176 | 3246 | 3188 |
| Longitudinal Wave | 5698 | 5639 | 5612 | 5640 | 5647 |

Recall the equations in last chapter. Rayleigh wave velocity and transvers wave velocity can be calculated through elastic constants (Eq.3-30). In the other hand, elastic constants can be obtained by measured velocities. Then I used all experimental data to calculate the elastic constants shown below. The measured modulus of elasticity matches the known value well.

Table 5-3 Experimental Elastic Constant

| c_R/c_T | Density, $\rho(g/cm^3)$ | Poisson's Ratio, μ | Modulus of Elasticity, $E(GPa)$ |
|-----------|-------------------------|------------------------|---------------------------------|
| 0.917 | 7.76 | 0.231 | 194.17 |

5.2 ROUGHNESS

Since Rayleigh wave much depends on surface condition. Testing on different roughness is necessary. In this section, to make a uniform rough surface, grinding papers have been used (60, 320, 1200). To have a better understanding of roughness condition, optical profiler was applied. All the surface pictures and waveform tested results are plotted below.

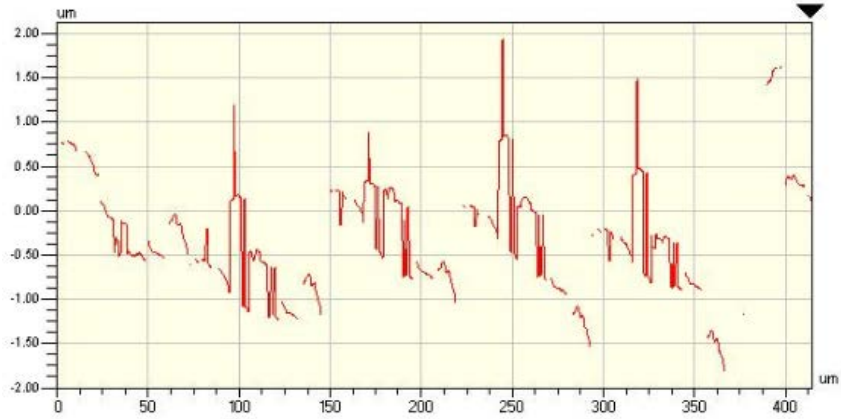


Figure 5-12 2D Analysis on #60 Sample x-axis

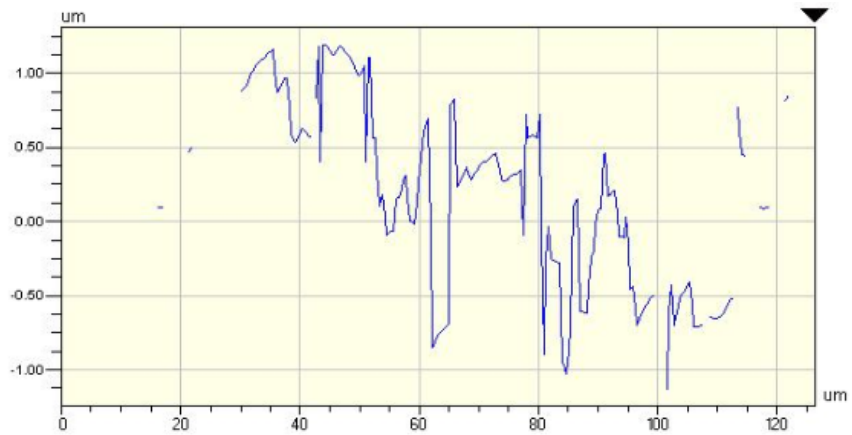


Figure 5-13 2D Analysis on #60 Sample y-axis

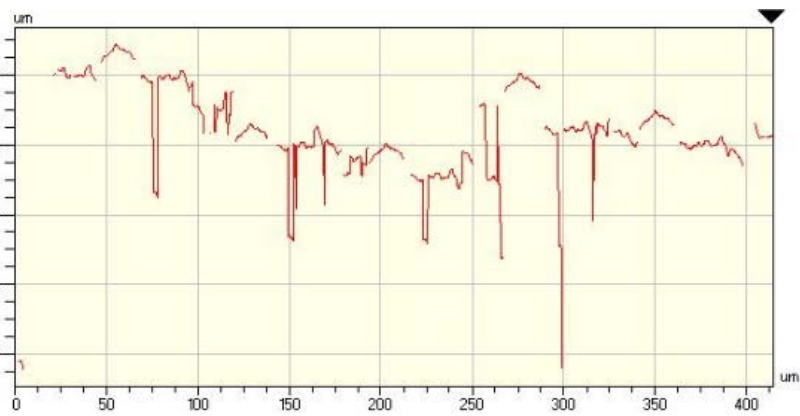


Figure 5-14 2D Analysis #320 Sample x-axis

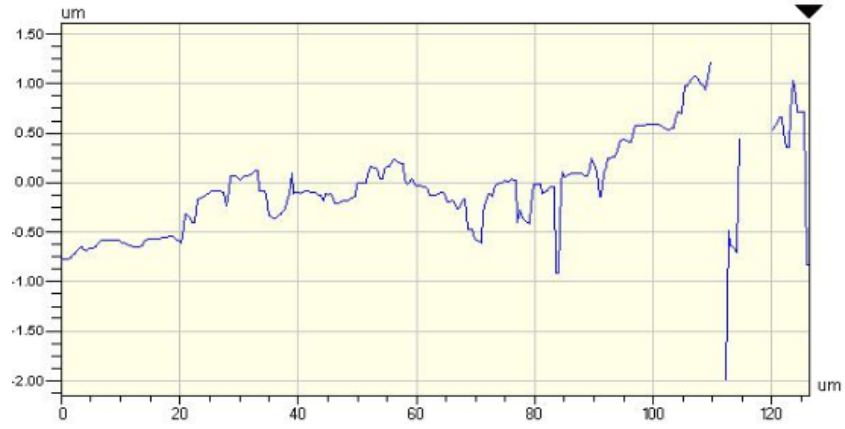


Figure 5-15 2D Analysis #320 Sample y-axis

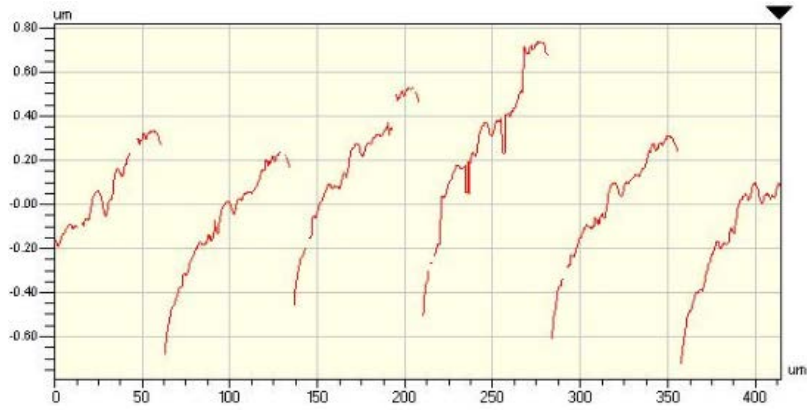


Figure 5-16 2D Analysis #1200 Sample x-axis

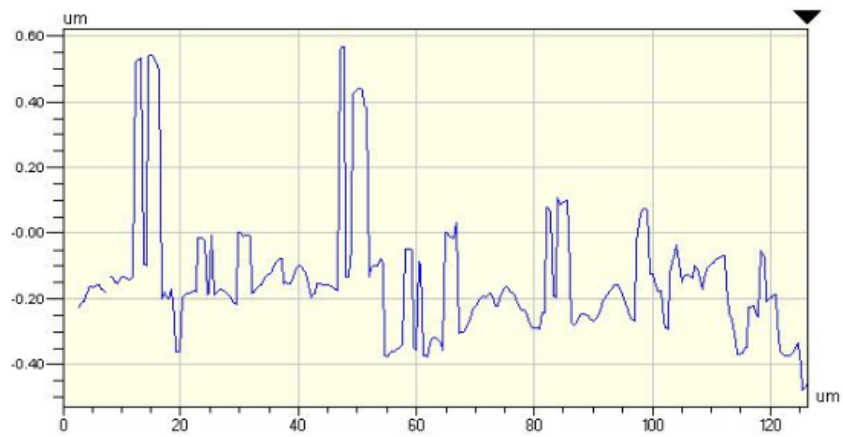


Figure 5-17 2D Analysis #1200 Sample y-axis

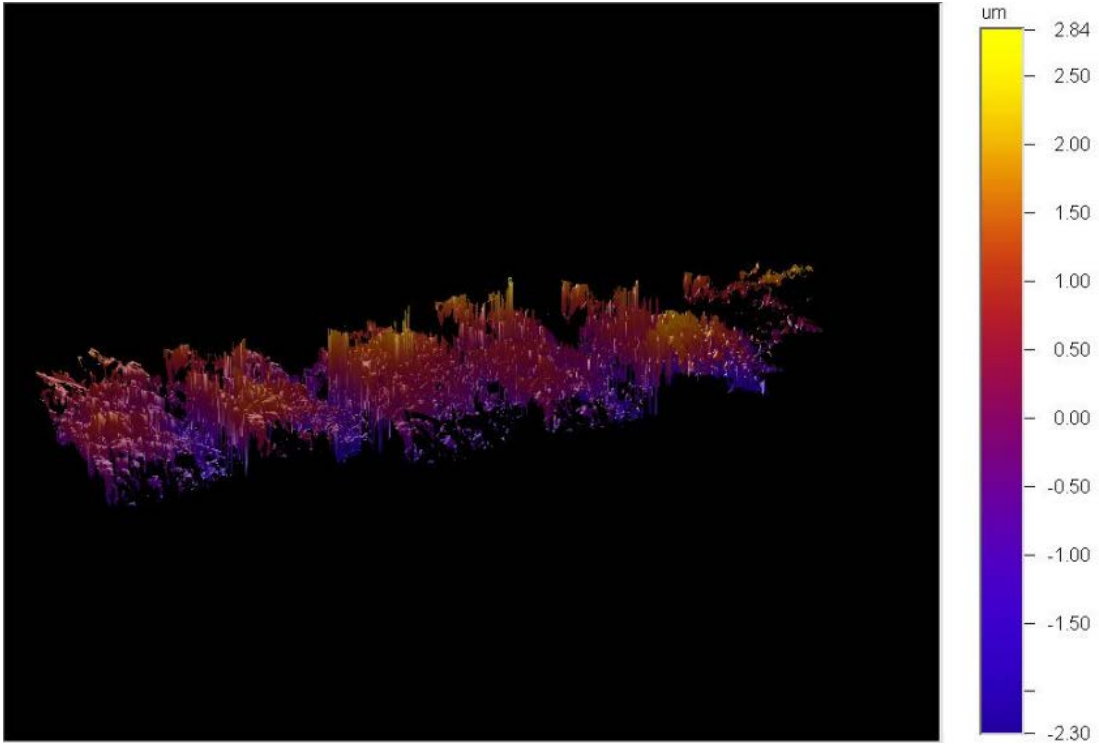


Figure 5-18 3D Interactive Display #60 Sample

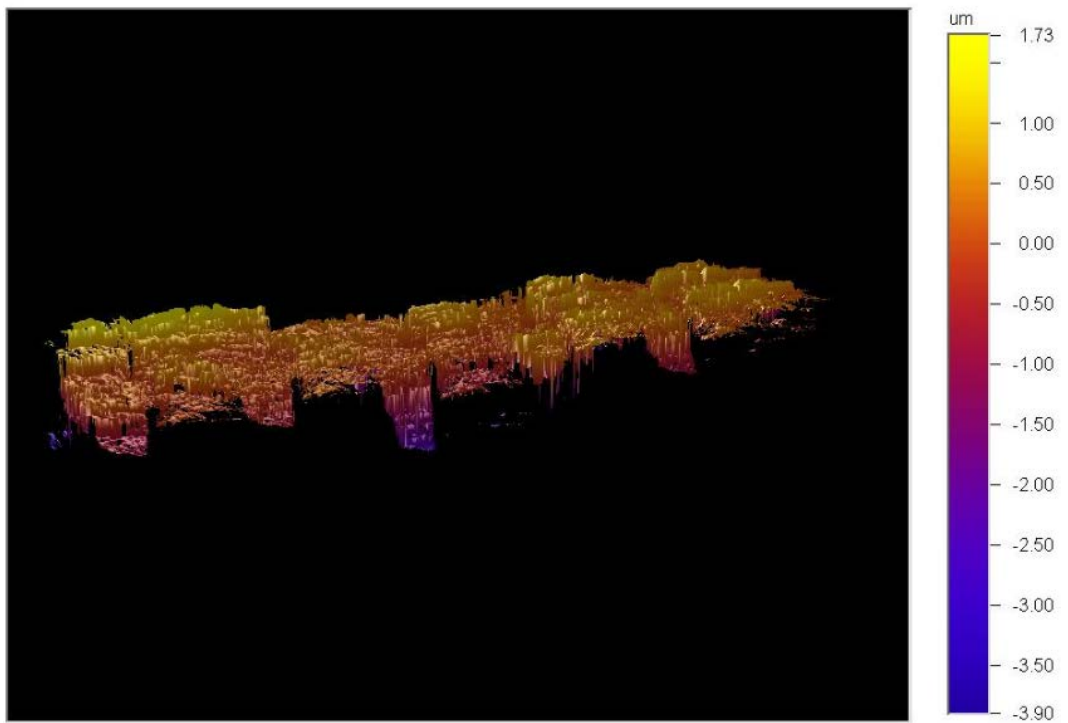


Figure 5-19 3D Inactive Display #320 Sample

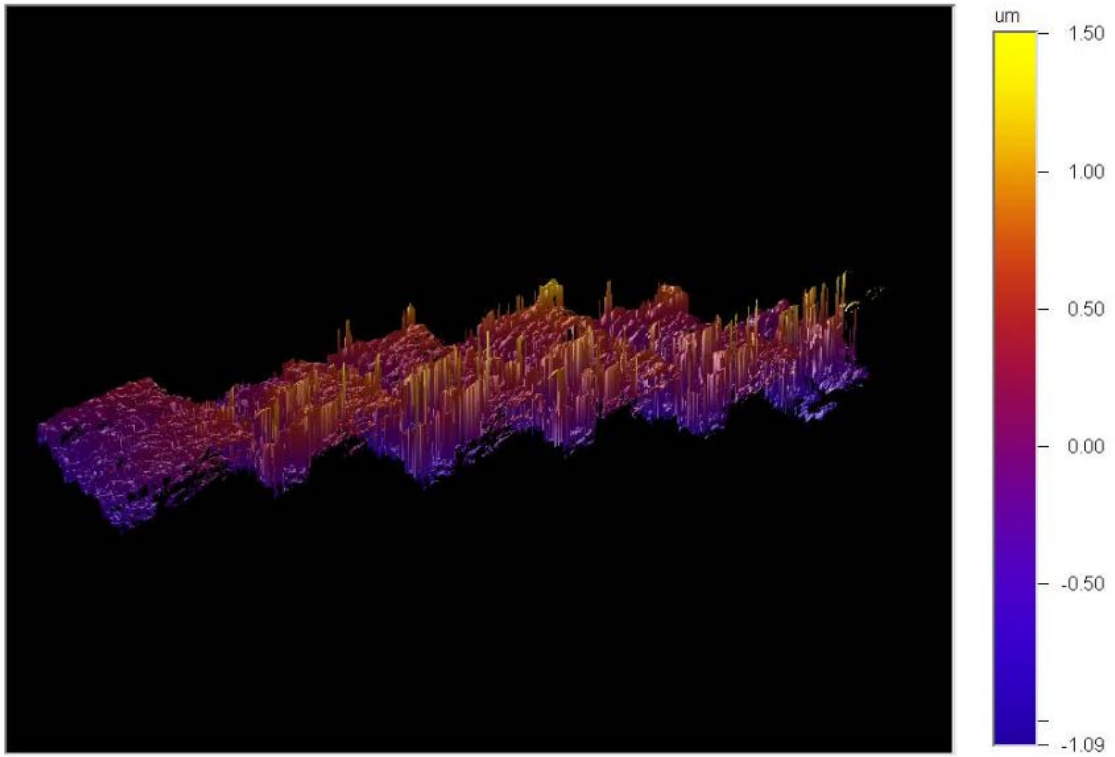


Figure 5-20 3D Interactive Display #1200 Sample

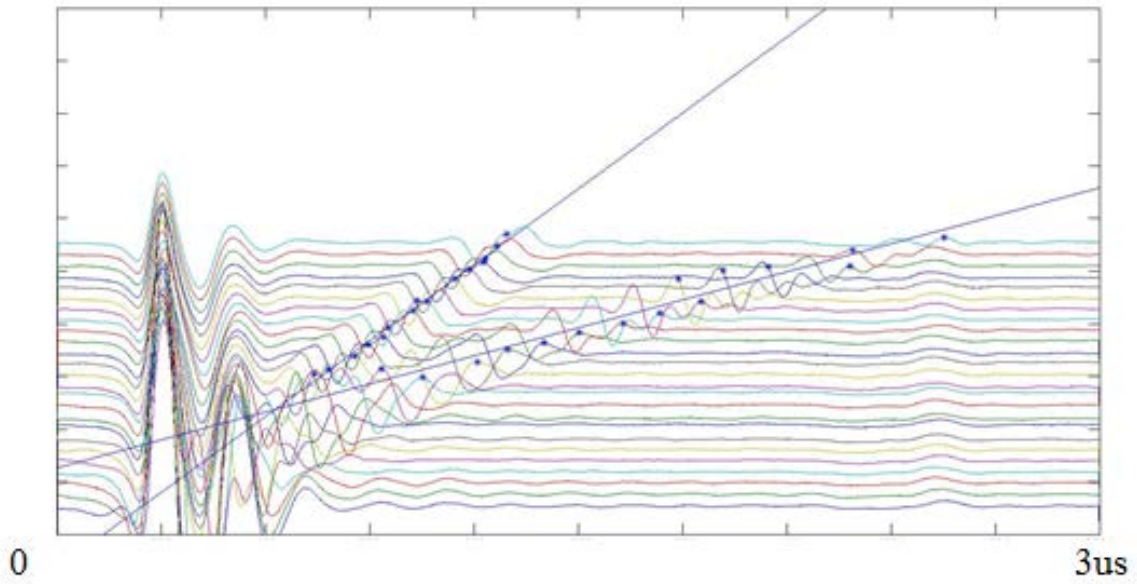


Figure 5-21 Sample polished with grinding paper 60

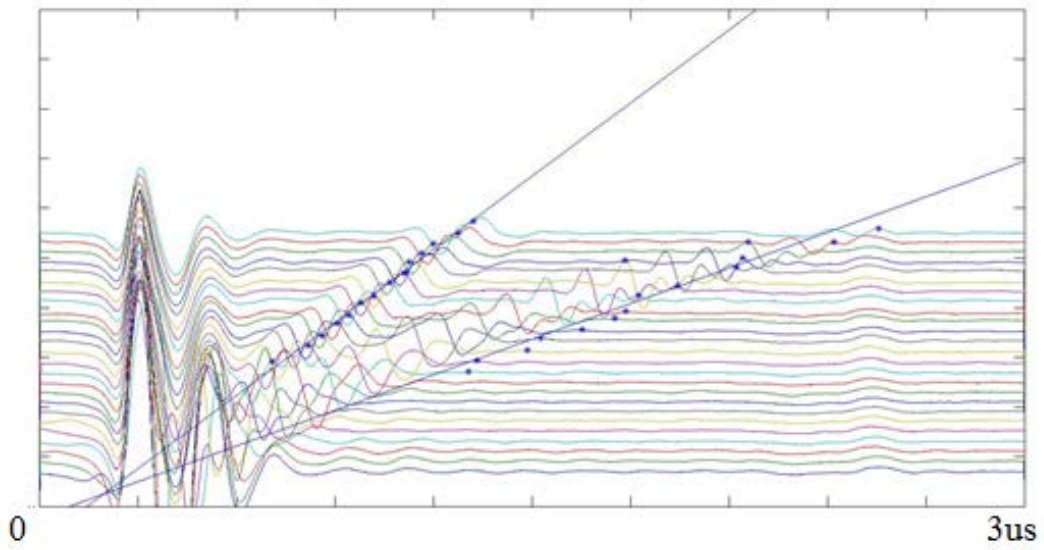


Figure 5-22 Sample polished with grinding paper 320

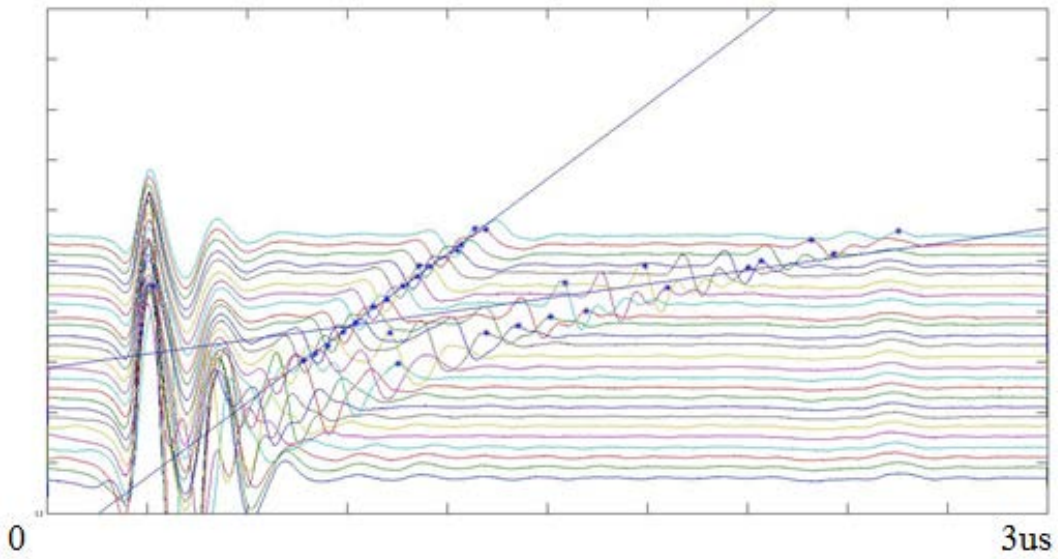


Figure 5-23 Sample polished with grinding paper 1200



Figure 5-24 Wave Velocities on Different Roughness Surface Comparison

Table 5-4 Elastic Constants Calculated from Roughness Testing Results

| | c_R/c_T | Poisson's Ratio, μ | Modulus of Elasticity, E (GPa) |
|---------------------|-----------|------------------------|----------------------------------|
| Grinding Paper 60 | 0.918 | 0.240 | 189 |
| Grinding Paper 320 | 0.920 | 0.249 | 184 |
| Grinding Paper 1200 | 0.912 | 0.205 | 171 |

In this section, the velocities did deduce on rough surface. However, because I did not gain a certain relationship between roughness and wave velocities, elastic constants calculated from different roughness samples were also not satisfying.

5.3 ADDITIVE MANUFACTURING PRODUCTS

5.3.1 ExOne M-Flex

In M-Flex additive manufacturing process, raw parts printed are stick together by the chemical binder and fragile. After printing, sintering is the process which solidify the raw parts [29].

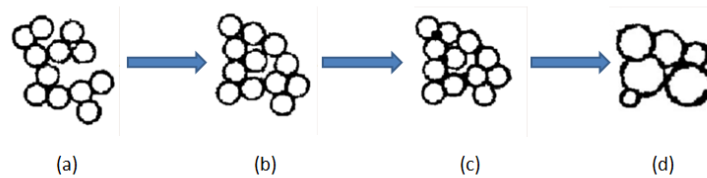


Figure 5-25 Illustration of Partical Sintering

Sintering, in a simple way to say, is rising the temperature to reach 70% - 80% of melting point to make particles attach to each other, in order to solidify the part. Sintering profile, which describes the heating temperature, heating time, and even increasing/decreasing rate of temperature.

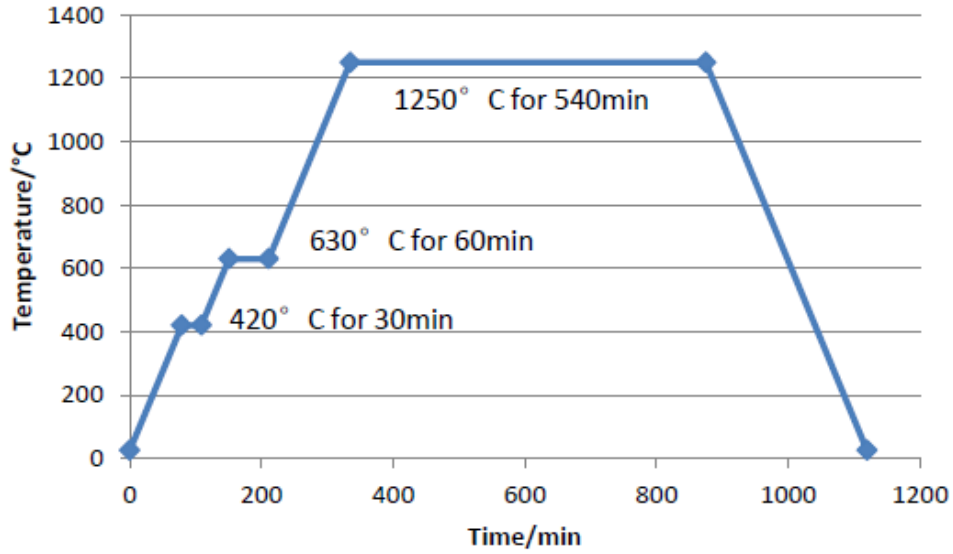


Figure 5-26 A kind of Temperature Profiles during Sintering[29]

In my work, ultrasonic wave testing was applied on sintering parts processed by different heating profile. After sintering, pores on the surface still exist. Optical profiling method was applied to measure the surfaces as well.

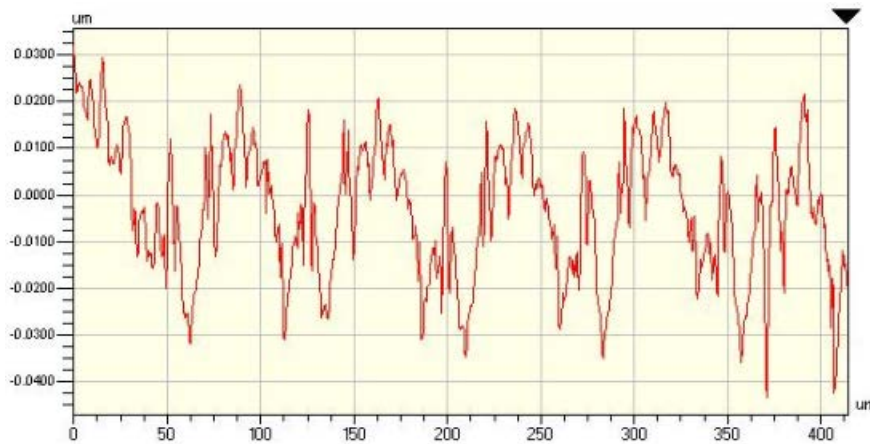


Figure 5-27 2D Analysis x- axis on Sample 150 mins at 1375 degree

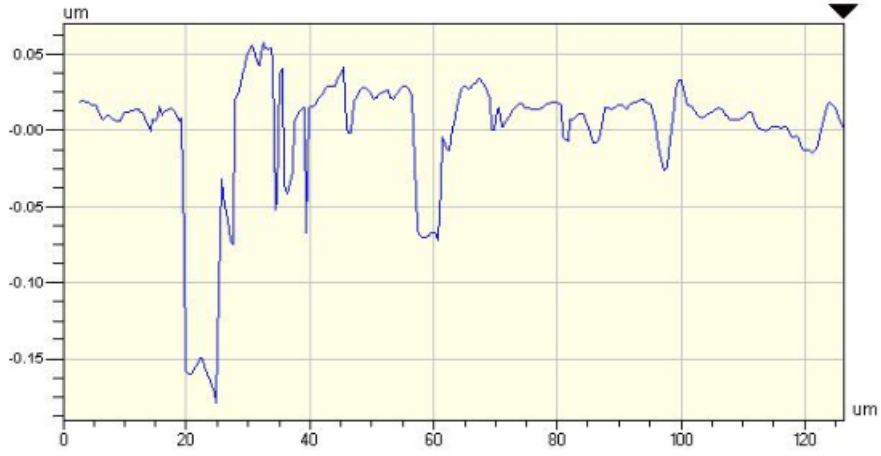


Figure 5-28 2D Analysis y-axis on Sample 225 mins at 1375 degree

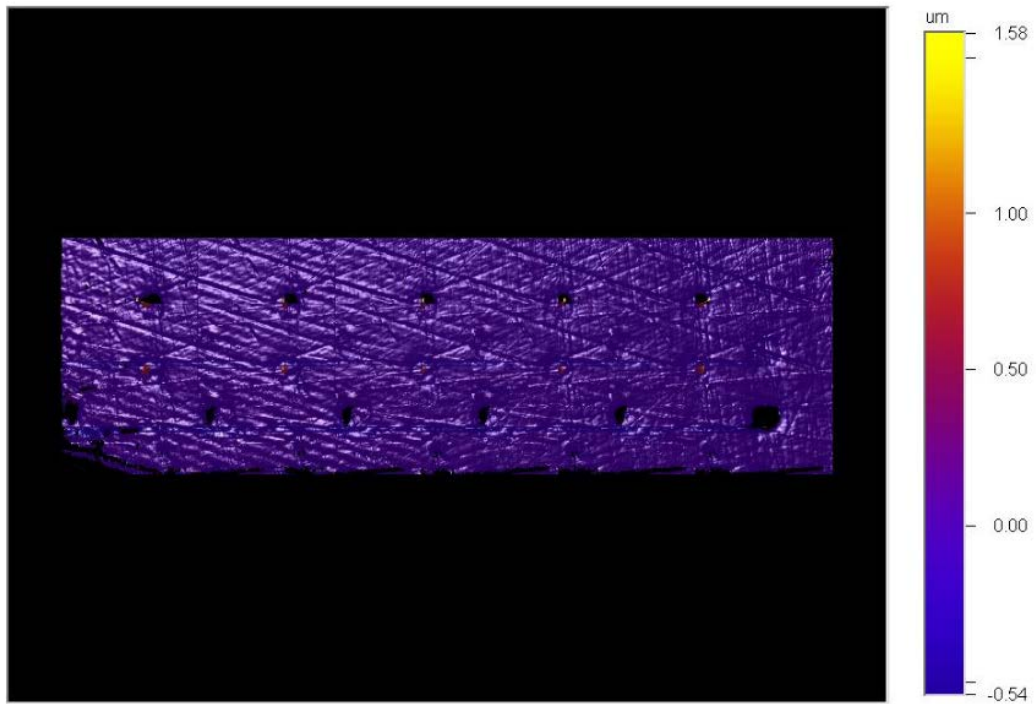


Figure 5-29 3D Interactive Display of Sample 150 mins at 1375 degree



Figure 5-30 2D Analysis x- axis on Sample 225 mins at 1375 degree

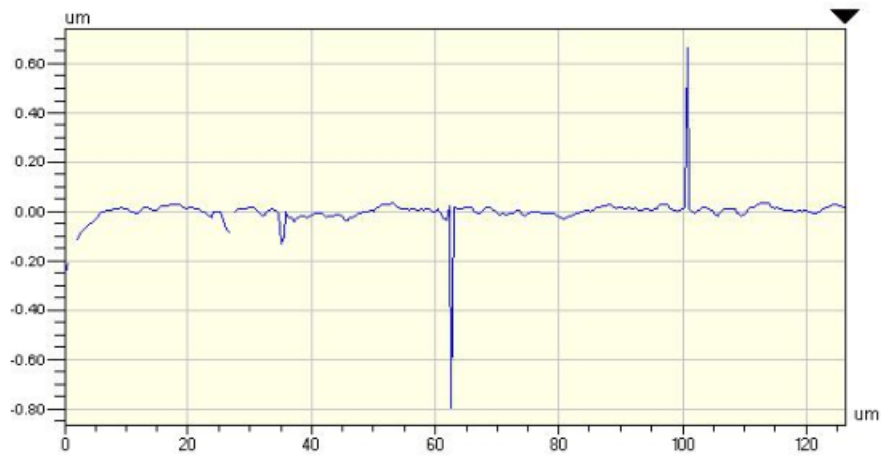


Figure 5-31 2D Analysis y- axis on Sample 225 mins at 1375 degree

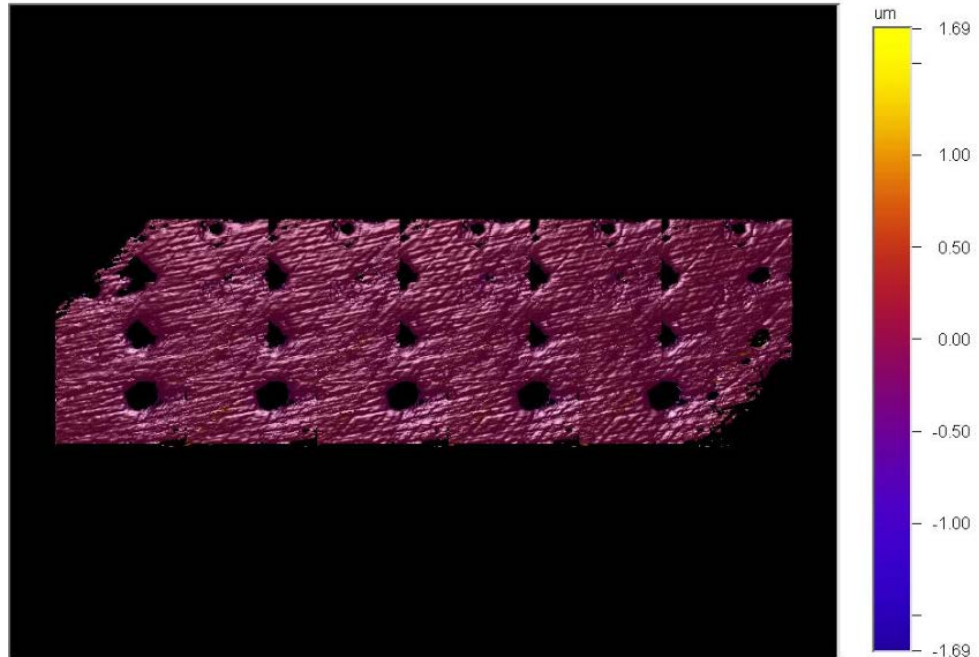


Figure 5-32 3D Interactive Display of Sample 225 mins at 1375 degree

Unfortunately, sample under heating profile (1350°C at 300mins) could not be focused by optical profiler. In ultrasonic wave testing, three different samples fabricated under different sintering profiles were measured, and then elastic constants were calculated instantly.

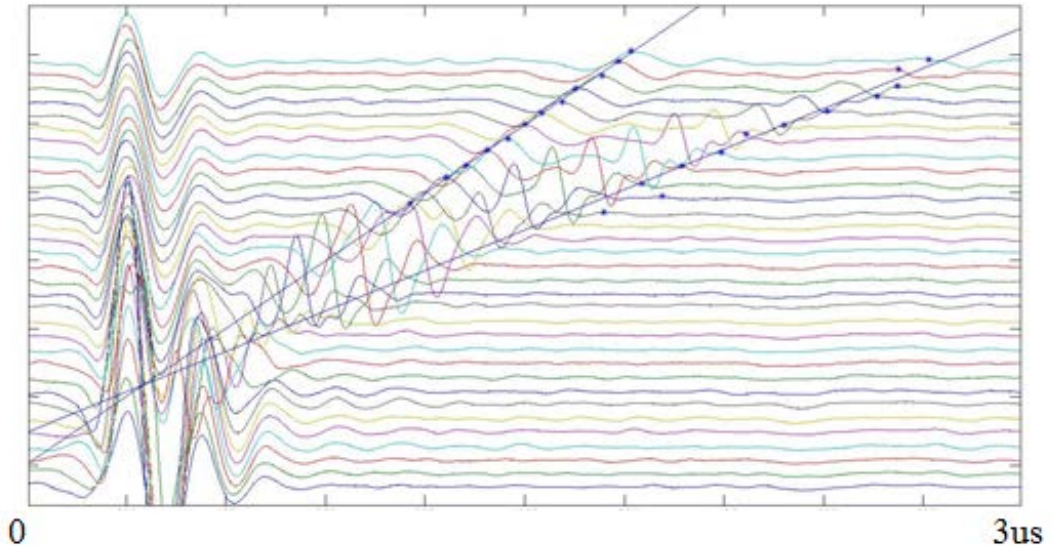


Figure 5-33 Sintering Process at 1350 degree for 300 mins

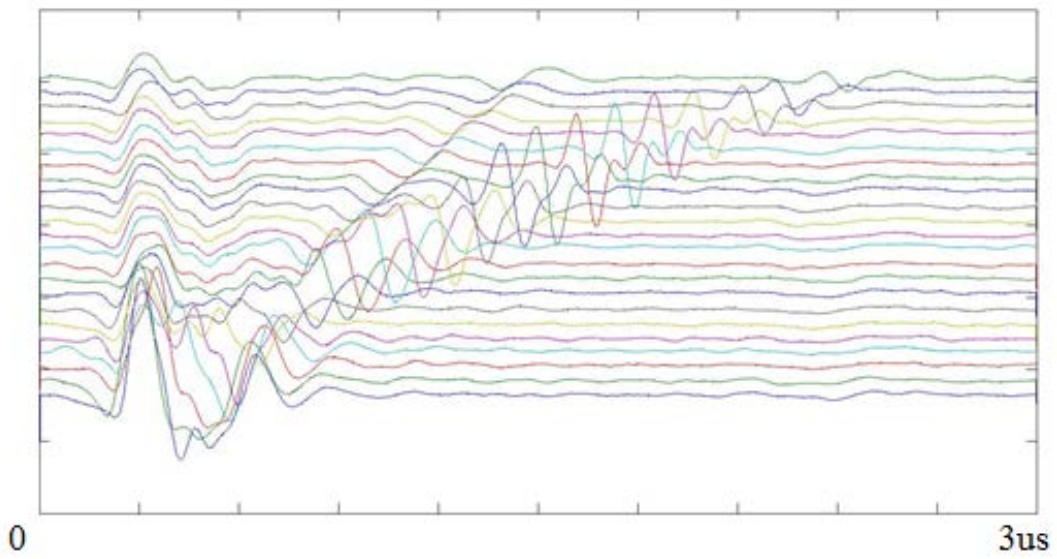


Figure 5-34 Sintering Process at 1375 degree for 225 mins

Table 5-5 Elastic Constants Calculated by Ultrasonic Wave Testing Method

| | Density, $\rho(g/cm^3)$ | c_R/c_T | Poisson's Ratio, μ | Modulus of Elasticity, $E(GPa)$ |
|----------------------|----------------------------|-----------|------------------------|------------------------------------|
| 1350°C at 300mins | 6.74 | 0.940 | 0.389 | 160.80 |
| 1375°C at 150mins | 7.17 | N/A | N/A | N/A |
| 1375°C at 225mins | 7.22 | 0.925 | 0.281 | 209.43 |

I could draw the slop in sample with sintering profile (1375°C at 150mins). As a result, only two other samples have been tested successfully.

5.3.2 LENS 450 Laser 3D Printer

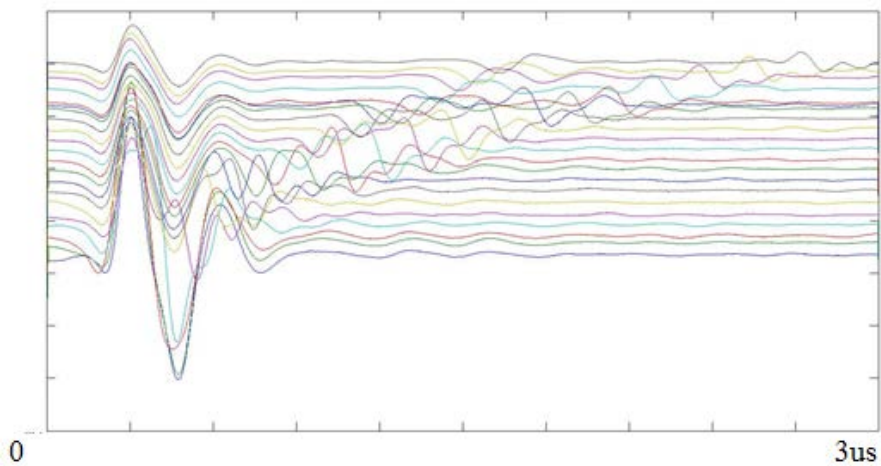


Figure 5-35 Waveforms of Laser Sample with offset

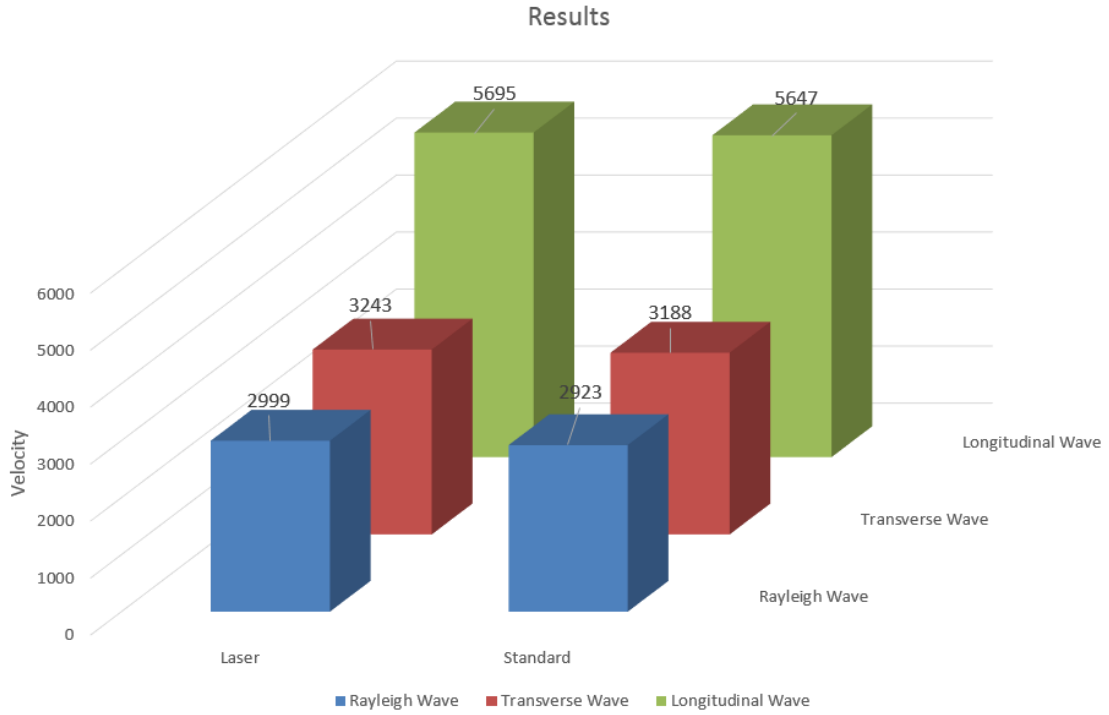


Figure 5-36 Comparison between Laser Additive Manufacturing Sample and Standard Sample

Table 5-6 Elastic Constant Results of Laser Additive Manufacturing

| | Density, $\rho(g/cm^3)$ | c_R/c_T | Poisson's Ratio, μ | Modulus of Elasticity, $E(GPa)$ |
|-------|----------------------------|-----------|------------------------|------------------------------------|
| Laser | 7.78 | 0.917 | 0.23 | 201.40 |

6.0 CONCLUSION AND FUTURE WORK

6.1 CONCLUSION

This Rayleigh wave testing method has been proved successful and accurate in control group.

All the elastic constants calculated from experimental data matched official data well.

Additive manufacturing products still need improvement. Laser additive manufacturing method showed the best sample performance. Elastic constants measured by tensile test also matched the results in ultrasonic wave testing.

6.2 FUTURE WORK

6.2.1 Different Piezoelectric Material

Commercial PVDF material has some advantages: small piezoelectric charge (useful for actuators) and large voltage constants (g, good for sensors), etc. Thin sheets of PVDF can be stretched in one direction or in two, perpendicular, directions along the plane of the sheet, then formed into almost any shape. However, PZT and other piezoelectric material exhibits much higher other characters, then more materials will be applied in experiments.

Table 6-1 Piezoelectric Properties of PVDF and Piezoelectric Ceramics

| Property | Units | PVDF | BaTiO₃ | PZT |
|-----------------------------------|--|---|--------------------------|------------------------------|
| Dielectric Constant | pC/N | 12 | 600 - 1200 | <1000 - 4000 |
| Piezoelectric Charge Constant | | d ₃₁ = 20 d ₃₃ = -30 | -30 - -60 <100 - 150 | ~-100 - >-600 ~200 - >600 |
| Electromechanical Coupling Factor | % | 11 | 21 | 30 - 75 |
| Young's Modulus | 10 ¹⁰ N/m ² | 0.3 | 11 - 12 | 6 - 9 |
| Acoustic Impedance | 10 ⁶ kg/(m ² s)* | 2.3 | 25 | 30 |
| Density | Kg/m ³ | 1780 | 5300 - 5700 | 7500 - 7700 |

6.2.2 Anisotropic Material Characterization

In this article, stainless steel, an isotropic material, was characterized by ultrasonic wave testing method. This Rayleigh wave characterization method would also applicable on anisotropic material which has different modulus in different direction.

APPENDIX

FUNDAMENTAL OF PIEZOELECTRIC

Here is the relationship between physical energy and electrical energy:

$$P = D - \varepsilon^T E$$

where P is polarization, D is electric displacement, ε^T is permittivity of ceramic at constant stress, E is electric field

Piezoelectric Relative Constants & Equations

- Piezoelectric Charge Constant d_{xy}
- Frequency Constant
Resonance frequency (linear dimension governing resonance)

$$N_L: \text{longitudinal mode} \quad N_L = f_s l$$

$$N_P: \text{radial mode} \quad N_P = f_s D \phi$$

$$N_T: \text{thickness mode} \quad N_T = f_s h$$

BIBLIOGRAPHY

- [1] Mark V. Brook. *Ultrasonic Inspection Technology Development and Search Unit Design: Examples of practical applications*. IEEE Press.2011
- [2] *Piezoelectric Ceramics: Principles and Applications*. APC international Ltd.
- [3] Yu Zhou. *Characterization of the Porosity and Pore Behavior During the Sintering Process of 420 Stainless Steel Samples Produced with Gas- and Water- Atomized Powder Using Powder Based 3-D Printing*. University of Pittsburgh, 2011
- [4] Lester W. Schmerr, Jr. *Fundamentals of Ultrasonic Nondestructive Evaluation, A Modeling Approach*. Plenum Press, New York, 1998.
- [5] Lord Rayleigh. *On Waves Propagated Along the Plane Surfaces of An Elastic Solid*. London Math Society, 17, 1885
- [6] E. Naryshkina. *General Theory of Rayleigh Waves for a Half-Space*. Trudy Seismologicheskogo Instituta Akad, Nauk SSSR, No. 90, 1940
- [7] J.D. Achenbach, A. K. Gantesen, H. McMaken. *Ray methods for Waves in Elastic Solids*. Pitman, Boston, 1982
- [8] J.D. Achenbach. *Wave Propagation in Elastic Solids*. American Elsevier, New York, 1973
- [9] Warren P. Mason, R. N. Thurston. *Physical Acoustics, Principles and Methods*. Volume X. Academic Press, Inc, 1973
- [10] J. David, N. Cheeke. *Fundamentals and Applications of Ultrasonic Waves*. CRC Press, 2nd Edition
- [11] Igor Aleksandrovich Viktorov. *Rayleigh and Lamb Waves: Physical Theory and Applications*. Plenum Press, New York, 1967.
- [12] R.A. Lemons, C. F. Quate. *Acoustic Microscope-Scanning Version*. Microwave Laboratory, Stanford University, 1973

- [13] W. Parmon, H. L. Bertoni. *Ray Interpretation of the Material Signature in the Acoustic Microscope*. Electronics Letters, Vol. 15, No. 21, 1979
- [14] Abdullah Atalar. *A Physical Model for Acoustic Signatures*. Journal of Applied Physics, 1979
- [15] A Briggs. *Acoustic Microscope*. Oxford University Press, 2009
- [16] Kushibiki J, Ishiji H. *Material Characterization by Line-Focus-Beam Acoustic Microscope*. IEEE Transactions on Sonics and Ultrasonics, Volume SU-32, 1985
- [17] Kushibiki J, Ishiji H. *Characterization of 36/spl deg/YX-LiTaO/sub 3/wafers By Line-focus-beam Acoustic Microscopy*. IEEE Transactions on Ultrasonics, Ferroelectrics, and Frequency Control, Vol. 42, 1995
- [18] Dan Xiang, N.N. Hsu, G.V. Blessing. *The Design, Construction and Application of a Large Aperture Lens-Less Line-Focus PVDF Transducer*. National Institute of Standard and Technology, 1996.
- [19] Ross A. Lemons, Calvin F. Quate. *A Scanning Acoustic Microscope*. Stanford University, 1973
- [20] Calvin Quate, Abdullah Atalar, H. K. Wickramasinghe. *Acoustic Microscopy with Mechanical Scanning-A Review*. Proceedings of the IEEE, Vol.67, No. 8, August 1979
- [21] A. Atalar, C.F. Quate, H. K. Wichramasinghe. *Phase imaging in reflection with the acoustic microscope*. Applied Physics Letters, 1977
- [22] Yung-Chun Lee, Jin O. Kim, and Jan D. Achenbach. *Acoustic Microscopy Measurement of Elastic Constants and Mass Density*. IEEE Transactions on Ultrasonics, Ferroelectrics, and Frequency Control. Vol. 42, No. 2, March 1995
- [23] M. Born, E. Wolf. *Principles of Optics*. 7th edition Cambridge Pergamon Press, 1999
- [24] L.H. Brekhovskikh. *Waves in Layered Media*. Academic Press, Inc. 1980
- [25] American Society for Testing and Materials(ASTM) E 1316-10b
- [26] Holler F. James, Douglas Skoog. *Principle of Instrumental Analysis*. Cengage Learning, Chapter 1, 2007
- [27] G. Lippmann. *Principe de la conservation de l'électricité*. Annales de chimie et de physique (in French) 24: 145.
- [28] J. Kushibiki, Y. Ono, Y. Ohashi, M. Arakawa. *Development of the Line-Focus-Beam Ultrasonic Material Characterization System*. IEEE Transactions on Ultrasonics and Frequency Control, Vol. 49, No. 1, Jan 2002

- [29] Yu Zhou. *Characterization of The Porosity and Pore Behavior During the Singtering Process of 420 Stainless Steel Samples Produced with Gas- and Water- Atomized Powder Using Powder Based 3-D Printing*. University of Pittsburgh, 2014
- [30] T. Mihara, M. Obata. *Elastic Constant Measurement by Using Line-Focus-Beam Acousitc Microscope*. Experimental Mechanics, p33, 1992
- [31] L.M. Brekhovshikh. *The Propagation of surface Rayleigh waves along the uneven surface of an elastic solid*. Akust, 5(3):282-289, 1959.
- [32] L, Bergmann. *Der Ultraschall*, 6. Aufl. Hirzel 1954
- [33] Ross A. Lemons, Calvin F. Quate. *Acoustic Microscopy*. Academic Press, Inc. 1979